Oral administration of Manuka honey modulates gut microbiota composition and enhances anti-tumor immunity in a preclinical model of colorectal cancer

Razan J. Masad
United Arab Emirates University, College of Medicine & Health Sciences
Ghada Bashir
United Arab Emirates University, College of Medicine & Health Sciences
Ashraf Al-Sbiei
United Arab Emirates University, College of Medicine & Health Sciences
Yassir A. Mohamed
United Arab Emirates University, College of Medicine & Health Sciences
Farah Al-Marzooq
United Arab Emirates University, College of Medicine & Health Sciences
Abeer Al-Tahrawi
United Arab Emirates University, College of Medicine & Health Sciences
Maria J. Fernandez-Cabezudo
United Arab Emirates University, College of Medicine & Health Sciences
Basel K. al-Ramadi (ramadi.b@uaeu.ac.ae)
United Arab Emirates University, College of Medicine & Health Sciences

Research Article

Keywords: Manuka honey, cancer prevention, immunomodulation, Type I/II IFN, tumor microenvironment, colorectal cancer

Posted Date: August 24th, 2023

DOI: https://doi.org/10.21203/rs.3.rs-3273451/v2

Abstract

Conclusions: Our findings demonstrate that oral administration of MH induces specific alterations in the gut microbiota and triggers innate and adaptive mucosal immune responses through the activation of type I/II IFN signaling pathways. This culminates in rendering the tumors more immunogenically responsive. Our data highlight the immunostimulatory properties of MH and demonstrate its potential utilization in cancer prevention.

Background: There is increasing interest in exploring alternative natural products for cancer prevention and treatment. Among these, we recently highlighted the potential utilization of Manuka honey (MH) as an immunomodulatory agent. In the present study, we characterized mechanistically the immunomodulatory properties of MH in a preclinical model of colorectal cancer (CRC).

Methods: MH was administered orally over a 4 week-period. A solution containing equivalent concentrations of the main sugars in MH was used as a control (SC). Mucosal and systemic lymphoid tissues were examined for alterations in cellular composition and activation status by multi-color flow cytometry (FACS). Fecal pellets were collected before and after treatment and used for bacterial 16S rRNA sequencing. Pretreated mice were implanted with CRC cells and followed for tumor growth. Tumors, lymph nodes, and spleens were analyzed by FACS, immunohistochemistry, and qRT-PCR 3-weeks post-implantation.

Results: Pretreatment with MH, but not SC solution, induced type I/II IFN response in mucosal and systemic lymphoid tissues, resulting in enhanced expression of IFN-inducible stem cell antigen-1 (Sca-1) and MHC class II proteins. In an implantable model of CRC, tumor growth was significantly retarded in MH-pretreated mice. These tumors had increased infiltration of immune cells, ~2.0-fold increase in the percentage of intratumoral $CD4^+$ and $CD8^+$ T cells, and a 50% decrease in the percentage of $Ly6G^+$ myeloid cells. Immunohistochemical analysis of tumor tissues revealed an increase in $CD4^+$ and $CD8^+$ T cells and granzyme-B-expressing cells following MH treatment. Moreover, FACS analysis showed significantly elevated expression of MHC class I on tumors of MH-treated mice. qRT-PCR analysis of purified tumor-infiltrating leucocytes highlighted changes in the expression of various chemokines and inflammatory cytokines that underlie the increased tumor immunogenicity. Finally, bacterial 16S rRNA sequencing revealed unique enrichment of >20 bacterial genera in MH-treated mice.

INTRODUCTION

Cancer represents a crucial global health concern, accounting for 10 million deaths annually [1]. Cancer growth results from a multistep process during which cells acquire multiple mutations, eventually leading to continuous cellular growth and division. Although several factors can contribute to cancer development, a compromised immune system is widely recognized as a dominant contributor to the onset and progression of cancer [2,3].

The role of the immune system in cancer is illustrated by its ability to eradicate emerging transformed cells once they arise, a concept known as “cancer immunosurveillance” [4]. However, tumor cells are capable of acquiring characteristics and strategies by which they can evade the immune system and consequently progress in their growth [5]. In light of the vital role of the immune system in cancer development and progression, there is a rising interest in employing cancer immune preventive agents to amplify immune responses and reduce cancer susceptibility in healthy individuals.

There is a growing body of evidence suggesting that different types of honey have anti-cancer properties [6]. Previously, our lab and others demonstrated the potential of Manuka honey (MH) to impede the growth of various types of human and murine cancer cell lines [7–9] and revealed the underlying molecular mechanisms of its anti-tumor action [8,10]. MH has also been described to possess immunomodulatory properties [11]. While some studies highlighted the potential of MH as an anti-inflammatory agent [12,13], others demonstrated that MH also exhibits pro-inflammatory properties [14–19].

In our previous work, we demonstrated that MH can trigger the activation of macrophages by inducing the expression of various pro-inflammatory cytokines and chemokines [15]. Additionally, when administered intraperitoneally, MH elicited a peritoneal immune response characterized by a significant increase in the recruitment of neutrophils and an enhancement in the functional maturation of peritoneal macrophages [15]. In the present study, we investigated the effect of oral administration of MH on the host immune system and its potential to modulate anti-tumor immune responses in an implantable murine colorectal cancer (CRC) model. Several reports demonstrated that alterations in the composition of gut microbiota and their translocation to secondary lymphoid organs can stimulate immune responses against tumors by influencing various cell types such as $CD8^+$ and $CD4^+$ T cells as well as tumor-associated myeloid cells [20,21]. Therefore, we also assessed the potential changes in microbiota composition following MH treatment in this study. Our findings provide compelling evidence that supports a role for MH as an immunomodulatory anti-tumor agent, highlighting its potential use in cancer prevention.

MATERIALS and METHODS

Cell line and Reagents

The murine CT26 colon carcinoma cell line was a kind gift from Dr. Siegfried Weiss (Helmholtz Centre for Infection Research, Braunschweig, Germany). Cells were maintained as previously described [9]. Manuka honey (UMF® 20+ from ApiHealth, Auckland, New Zealand) was used in the current study and diluted in distilled water under aseptic conditions. As a control for MH, a sugar solution, designated sugar control (SC), containing equivalent concentrations of the three major sugars (Sigma, St. Louis, MO, USA) in honey (38.2% fructose, 31.3% glucose, and 1.3% sucrose) was used [8].

Experimental animals

BALB/c mice were purchased from the Jackson Laboratory (Bar Harbor, ME, USA). All animals were bred in the animal facility of the College of Medicine and Health Sciences, United Arab Emirates University. For the current study, male mice at the age of 8–10 weeks were used. Mice received rodent chow and water ad libitum. All studies involving animals were carried out in accordance with, and after approval of the Animal Research Ethics Committee of the United Arab Emirates University (Protocols #A12-13 and ERA-2019-5853).

Oral treatment and tumor studies

BALB/c mice of comparable age and weight were randomly divided into two groups. Mice were gavaged daily with 0.2 mL of a water solution containing 70% SC or 70% MH (w/v). After 4 weeks of treatment, mice were euthanized, and their mesenteric lymph nodes (MLNs), inguinal lymph nodes (ILNs), and spleens were excised for further analysis.

In other experiments, mice were treated with SC or MH for 4 weeks, then subcutaneously inoculated with 2×10^5 CT26 cells in the right flank. Tumor dimensions (width and length) were measured using a digital caliper twice a week, and tumor volume was calculated using the formula: Tumor volume = $(L\times W^2)/2$, as detailed elsewhere [22,23]. Mice were euthanized 21 days post-implantation, and their tumors were excised for further analysis.

Processing of lymphoid organs and tumors

Single cell suspensions were prepared from the spleens, MLNs, and ILNs by mechanical dissociation as previously described [24]. Tumors were processed using a previously described method, with modification [25]. Briefly, dissected tumor tissues were subjected to mechanical and enzymatic digestion in gentleMACS C-tubes (Miltenyi Biotec, Germany) using a tumor dissociation kit (Miltenyi Biotec) and the GentleMACS dissociator (Miltenyi Biotec), according to manufacturer's instructions. Tumor-infiltrating leukocytes (TILs) were subsequently purified from tumor cell suspensions using magnetic $CD45^+$ microbeads and the autoMACS cell separator, according to the manufacturer's protocol (Miltenyi Biotec).

Flow cytometric analysis

Analysis of MLN, ILN, spleen, and tumor cells was carried out using multi-color flow cytometry, following our standard protocol [25,26]. The following antibodies (all purchased from Biolegend, San Diego, CA, USA) were used in the current study: anti-CD45-APC (Cat# 103112), anti-CD19-PE (Cat# 115508), CD19- PE-Texas Red (Cat# 115554), anti-CD3-BV785 (Cat# 100232), anti-CD4-FITC (Cat#

100509), anti-CD8-APC-Cy7 (Cat# 100714), anti-CD8-APC (Cat# 100712), anti-CD11b-Alexa Flour-488 (Cat# 101217), anti- CD11c-PE (Cat# 117308), anti- Ly6G-BV605 (Cat# 127639), Ly-6A/E (Sca-1)-PE-Texas Red (Cat# 108138), anti-MHC II (I-A/I-E)-BV785 (Cat# 107645), anti-MHC I H-2K^{d} -BV421 (Cat# 116623). Non-viable cells from tumors were excluded using 7-AAD viability dye (Biolegend) and non-viable cells from spleens, MLNs, and ILNs were excluded using Zombie Aqua dye (Biolegend). Data were collected on 10,000-50,000 cells (depending on the organ) using a FACSCelesta flow cytometer (BD Biosciences, Mountain View, CA, USA) and analyzed using FlowJo software (BD Biosciences).

Immunohistochemical analysis

Immunohistochemical staining was performed on tumor tissue sections as per established protocols in our laboratory [26,27]. Sections were incubated overnight with specific monoclonal antibodies to CD8 (ab209775; Abcam, UK), CD4 (ab183685; Abcam), or granzyme-B (44153S; Cell Signaling Technology, Danvers, MA, USA), after which they were incubated with HRP-conjugated goat polyclonal secondary antibody for 45 min at room temperature. Sections were then developed using DAB chromogen substrate (Dako, Carpinteria, CA, USA), counterstained with haematoxylin, and examined using an Olympus BX51 microscope (Olympus Corporation, Japan) at 40× magnification. The positive cells were counted in 10-20 randomly selected high-power fields (HPF), and the average count was calculated.

Quantitative real-time PCR

qRT-PCR was carried out essentially as previously detailed [25,26]. We used premade TaqMan primers and probes (Applied Biosystems, Foster City, CA, USA) for the following genes, CXCL1 (Mm04207460_m1), CXCL2 (Mm00436450_m1), CXCL10 (Mm99999072_m1), IFN-γ (Mm01168134_m1), and granzyme B (Mm00442834_m1). mRNA levels of target genes were normalized according to the comparative ΔCq method to respective mRNA levels of the housekeeping gene HPRT (Mm01545399_m1). The expression of the target gene is reported as the level of expression relative to HPRT and presented as fold change relative to control mice.

Fecal sample collection and DNA extraction

DNA was extracted from stool samples using the QIAamp Fast DNA Stool Mini Kit (Qiagen, Valencia, CA, USA), following standard protocol. DNA concentration was measured using the NanoDrop 1000 Spectrophotometer (ThermoFisher Scientific, Waltham, MA, USA).

Bacterial 16S rRNA gene amplicon Sequencing

16S Metagenomic Sequencing kit (Illumina, San Diego, CA, USA) was used for library preparation. V3–V4 hypervariable regions of the bacterial 16S rRNA gene were amplified using the primers (5'-CCTACGGGNGGCWGCAG-3' and 5' GACTACHVGGGTATCTAATCC-3') provided by the manufacturer and following the recommended protocol as described before [28]. Library concentration was assessed by Qubit Fluorometric Quantitation (Invitrogen, Waltham, MA, USA). Short-read paired-end amplicon sequencing was performed using Illumina® MiSeq Instrument for 600 cycles.

Bioinformatic analysis

Processing of sequencing reads (adaptor trimming and filtering of low-quality reads) followed by taxonomic classification were done using Quantitative Insights Into Microbial Ecology version 2 (QIIME2) software suite [29]. After the identification of Operational Taxonomic Units (OTUs), downstream analyses were carried out in RStudio (v 4.1.2). Diversity was measured using BiodiversityR (v 2.15-2) and plotted by ggplot2 (v. 4.1.3). Alpha diversity measures (Observed OUT, CHAO1, Shannon's Diversity, and Simpson's Diversity indices) were compared between the groups using Mann-Whitney U test. For beta diversity, principal coordinate analysis based on Jaccard and Bray Curtis dissimilarity metrics was used to assess differences between the groups using non-parametric multivariate analysis of variance (PERMANOVA). Linear discriminant analysis (LDA) effect size (LEfSe) was used to detect biomarkers from microbial profiles [30] using the Microbiome Analyst 2.0 platform (McGill, Canada), which was also used to generate the graph of relative abundance and the heatmap for groups comparison [31]. Venn diagrams were generated to compare the taxa exhibiting significant differences based on the LDA analysis for the identification of shared and unique OTUs [32].

Statistical analysis

All statistical analyses were performed using GraphPad Prism 9.0 (San Diego, CA, USA). Statistical significance between control and treated groups was determined using the unpaired, two-tailed Student's t-test. In all analyses, $p < 0.05$ was considered statistically significant * ($p < 0.05$), ** ($p < 0.01$), *** ($p < 0.001$) and **** ($p < 0.0001$).

RESULTS

Oral administration of MH induces functional alterations in host immune responses

We have previously demonstrated the ability of i.p. administration of MH to effect changes in the immune system via inducing the recruitment of neutrophils into the peritoneal cavity and the maturation of peritoneal macrophages [15]. In our efforts to apply a more physiological route of administration that would be safe and more applicable to humans, we investigated the effect of repeated oral administrations of MH on the immune system of BALB/c mice. Based on our previous experience, a

solution of 50-70% MH (w/v) is suitable for *in vivo* use in mice [9]. Naïve BALB/c mice were orally gavaged with water (control group), sugar control (SC) solution, or MH for 4 weeks. To address if repeated oral doses of MH are associated with any adverse events, body weights were determined in treated animals over the 4-week period. Baseline body weights were recorded before starting the treatment and at weekly intervals after treatment. The percentage change in body weight from baseline was then calculated. The results indicated that, in comparison with water-treated and SC-treated groups, treatment with MH over 4 weeks did not affect normal weight gain, with all 3 experimental groups showing comparable levels of body weight gain over the treatment period (Figure 1A). Accordingly, we selected SC as the control for all subsequent experiments. The potential effect of oral MH on blood glucose levels was also investigated by determining glucose levels in random blood samples collected on a weekly basis in SC or MH-treated mice. At the end of the treatment period, we observed that MH administration didn't alter the blood glucose levels, with both SC and MH groups showing comparable glucose levels that lie within the normal range (<200 mg/dL) (Figure 1B). Thus, no gross adverse effects were evident following oral administration of MH.

The capacity of MH to effect changes in the immune system was next investigated. Different peripheral lymphoid tissues including gut-draining MLNs, ILNs, and spleens were collected, and their weights and absolute cell counts were recorded. Our results indicated that MH administration did not alter the weights or the total cell counts of the collected tissues in comparison to SC-treated mice (Figure 1C-H). Furthermore, both vehicle-treated and SC-treated mice had comparable total weights and absolute cell counts in the peripheral lymphoid tissues tested (data not shown).

Next, multi-color flow cytometry was utilized to analyze the cellular changes in the collected tissues following MH administration. The gating strategy employed to identify the major immune subpopulations is shown in Supplementary Figure 1 (sFigure 1). FACS data indicated that MH administration did not lead to alterations in the cellular landscape of MLNs, ILNs, or spleens between SC or MH-treated mice (sFigure 2).

In the context of our previous findings demonstrating a functional maturation of macrophages that was observed following i.p. administration of MH, we next sought to investigate if similar alterations were induced following oral MH administration. Upregulation of MHC class II proteins on myeloid cells is a key event that is induced in response to activation through type I and/or type II interferon signaling pathways [33,34]. Therefore, we investigated whether oral administration of MH can induce any alterations within the cellular landscape of the peripheral lymphoid tissues, including MLN, ILN, and spleen. Given that the majority of cells in these tissues comprise T and B lymphocytes, we focused on analyzing changes in the expression of proteins known to be induced by type I/II IFNs. One of the well-known IFN-inducible genes is *Ly6a*, which encodes for Sca-1 protein on T lymphocytes [35–37]. The results of the flow cytometric analysis showed that oral administration of MH led to a significant increase in Sca-1 expression on both $CD8^+$ and $CD4^+$ T cells (Figure 2A). The percentage of Sca-1-positive $CD8^+$ T cells in MLNs, ILNs, and spleens increased by 21.6%, 24.4%, and 24.7%, respectively in MH-treated mice in comparison to SC-treated mice (Figure 2B, E, H). Similarly, the percentage of Sca-1-positive $CD4^+$ T

cells increased by 36.5%, 39.8%, and 62.9% in the same three organs, respectively (Figure 2C, F, I). These results show that oral MH administration induced IFN-dependent responses in T cells, both at the level of the gastrointestinal tract as well as in systemic lymphoid organs.

Oral administration of MH retards the growth of implanted tumors

The demonstration of the capacity of oral MH administration to activate T lymphocytes supports its potential role as an immunomodulatory agent. We reasoned that oral MH could potentially be used to boost immune responses preventatively in different disease settings. To test this hypothesis, we investigated the capacity of MH to modulate anti-tumor immune responses using an implantable murine CRC model. The treatment protocol followed in this study is illustrated in Figure 3A. Our findings revealed that pre-treating mice with MH resulted in a significant retardation of tumor growth. Tumors in mice given vehicle (H_2O) or SC solution grew continuously and rapidly, reaching a mean volume ± SEM of 897 ± 169 mm^3 and 916 ± 114 mm^3, respectively on day 21 post-implantation (Figure 3B). On the other hand, mice treated with MH exhibited a significant reduction in tumor volume, with a mean of 511 ± 90 mm^3 on day 21 post-implantation. The suppression in tumor growth was observed as early as 9 days post-implantation, and by day 21, it reached 44% compared to SC-treated mice (Figure 3B). These results highlight a potential immune-boosting anti-tumor role for MH when given preventively. It is worth noting that we have preliminary data showing a similar effect of MH in a second CRC model, namely MC38 tumors in C57BL/6 mice (data not shown).

MH treatment induces alterations within the tumor microenvironment

To investigate the underlying mechanism for the observed MH-mediated retardation of tumor growth, we analyzed the tumor microenvironment (TME) for alterations in the cellular landscape by flow cytometry. Tumors were excised at the end of the observation period, subjected to mechanical and enzymatic digestion, and processed to a single cell suspension. The cells were then stained with different panels of mAbs to quantify the cellular constituents within the tumor tissue. The gating strategies employed to identify the cellular subpopulations are illustrated in Supplementary Figure 3 (sFigure 3).

Tumor-infiltrating immune cells were identified by being positive for the pan-hematopoietic CD45 cell surface marker. There was a significant 36% increase in $CD45^+$ immune cells in the tumors of MH-treated mice compared to the control group (28% *vs.* 20%, respectively) (Figure 4A, B). FACS analysis revealed alterations in both the phenotypic and functional characteristics of the lymphoid and myeloid subpopulations in the TME. Regarding the $CD3^+$ T cell population, we observed a ~2-fold increase in the percentages of both cytotoxic $CD8^+$ T cells and helper $CD4^+$ T cells (Figure 4C-E) following MH treatment. The increase in the infiltration of T cells was also demonstrated morphologically by

immunohistochemistry, where the number of both $CD8^+$ and $CD4^+$ T cells was substantially increased in tumor tissue sections of MH-treated mice (Figure 4F-I).

Further analysis using myeloid cell-specific antibodies showed that the majority (70-80%) of the gated $CD45^+$ population in the TME were $CD11b^+$ myeloid cells. Interestingly, there was a significant decrease (~18%) in the percentage of intratumoral myeloid cells in the MH-treated group compared to the SC-treated group (Figure 5A, B). This was largely accounted for by a 50% reduction in the percentage of $Ly6G^+$ granulocytes (Figure 5C, D), most likely representing myeloid-derived suppressor cells [38]. In contrast, the percentage of $Ly6C^{hi}$ cells increased significantly (~1.7-fold) in MH-treated mice (Figure 5C, E). These cells have been described to be pro-inflammatory in function and are recruited to tumor tissue in response to CCL2/CCR2 signaling [39]. They further differentiate into MHC class II (MHC-II) positive or negative tumor-associated macrophages (TAM) dependent on macrophage colony-stimulating factor-mediated signals [40]. In terms of the other myeloid subpopulations, there was no major change in the percentages of $Ly6C^{lo/Neg}$ cells (Figure 5C, F) and dendritic cells ($CD11c^+$ cells) (Figure 5G, H) following MH treatment.

To gain insight into the functionality of intratumoral myeloid cells, we analyzed the level of expression of MHC-II proteins on $CD11b^+$ $Ly6G^-$ subpopulation. Interestingly, we observed a significant increase in both the percentage of myeloid cells expressing MHC-II proteins (2.4-fold) and the overall level of expression of MHC-II on these cells (3.0-fold increase in mean fluorescence intensity; MFI) in MH-treated group (Figure 6A-D), suggesting an enhancement in the antigen-presentation capacity of these cells within the TME.

Given the evidence of the involvement of type I/II IFN pathways in the observed functional changes in cellular function, we next analyzed whether similar alterations could be observed on the tumor cells. It is well known that the expression of MHC class I (MHC-I) proteins is regulated by type I/II IFN signaling pathways [41]. Therefore, we analyzed the expression of MHC-I proteins on $CD45^-$ tumor cells grown in mice after pretreatment with MH in comparison with tumor cells grown in control mice given SC solution. The results of this analysis showed that tumor cells grown in control mice showed bimodal levels of MHC-I expression, with 2 clearly discernible subpopulations being observed. The majority of these tumor cells (~62%) expressed low levels of MHC-I proteins, while the remaining population (~38%) showed high levels of MHC-I (Figure 7A-C). In sharp contrast, approximately 70% of tumor cells grown in mice pre-treated with MH exhibited high levels of MHC-I proteins (Figure 7A, C). Furthermore, a 7-fold increase in the MFI level of MHC-I proteins on tumor cells was observed following MH administration (Figure 7D, E). These results suggest that MH treatment enhanced the immunogenicity of tumor cells, rendering them more susceptible to killing by anti-tumor $CD8^+$ T effector cells. Taken together, our findings indicate that the ability of MH to effect changes in tumor growth is linked to a series of immunomodulatory alterations within the TME.

Altered expression of cytotoxic effector molecules and immunoregulatory chemokines following MH treatment

To elucidate the mechanism by which MH modulates the cellular components of the TME and exerts the observed anti-tumor response, RNA was extracted from purified $CD45^+$ hematopoietic cells of SC-treated and MH-treated mice, and the gene expression levels of key inflammatory chemokines and cytotoxic effector molecules were determined by qRT-PCR. MH treatment led to a ~1.6-fold increase in the expression levels of the CXCL10 chemokine, which is secreted in response to IFN-γ and preferentially regulates the recruitment of inflammatory T lymphocytes [42] (Figure 8A). Accordingly, the observed enhancement in the percentage of TILs following MH treatment could be attributed to increased expression of CXCL10. The expression levels of the CXCL2 and CXCL1 chemokines were also examined. Both of these inflammatory chemokines are potent chemoattractants that control the recruitment of polymorphonuclear leukocytes in inflammation and tissue injury [43]. qRT-PCR results indicated a substantial decline in the expression levels of CXCL2 (Figure 8B). A trend toward a decrease in the expression levels of CXCL1 was also observed (Figure 8C). These findings correspond with the observed reduction in the proportion of intratumoral $Ly6G^+$ granulocytes following MH treatment.

MH treatment also resulted in a significant increase in the expression levels of IFN-γ (~1.7-fold) and granzyme B (~2.8-fold) (Figure 8D, E), both of which are secreted by effector immune cells to induce apoptosis in tumor [44,45]. Consistent with these findings, immunohistochemical staining of tumor tissues indicated an increase in the number of granzyme B-positive cells following MH treatment (Figure 8F, G).

Collectively, these findings indicate that the MH-mediated suppression of tumor growth is facilitated by (1) an increase in the expression of CXCL10, leading to enhanced recruitment of T cells into the tumors of the mice; (2) a decrease in the expression of CXCL2 chemokine, resulting in reduced infiltration of granulocytes into the tumors of the mice; and (3) an upregulation in the expression of IFN-γ and granzyme B, ultimately leading to enhanced cytotoxic effects of the anti-tumor immune cells.

Oral MH induces changes in gut microbiota

We hypothesized that oral administration of MH could induce changes in gut microbiota that would underlie the enhanced anti-tumor immune responses observed in these mice. To address this possibility, we determined the composition of gut microbiota in fecal samples collected from mice either before treatment or after 4 weeks of treatment with MH or SC solution. Microbiota were profiled at the genus level to detect the alterations in abundance and diversity caused by each treatment. The stacked area plot (Figure 9) shows the relative abundances of genera ranked based on their prevalence in the samples (listed below in the graph) collected from mice before and after treatment with SC or MH. Variations were obvious among the samples. The microbiota fingerprint in the control group was maintained between week 0 and week 4. As for the MH group, microbiota profiles looked more homogenous after treatment

and with more similarity compared to the variability seen in week 0. To identify the genera with significant differences before and after each treatment, linear discriminant analysis (LDA) was done. As shown in Figure 10 (A and B), treatment with either SC or MH caused significant changes in microbiota profiles, with depletion of some genera (red color in the graphs) and enrichment of others (blue color in the graphs). These findings confirm that microbiota were changed after 4 weeks of either treatment. It is noteworthy that treatment with SC caused depletion of *Lactobacillus* which is generally considered a beneficial bacteria. In sharp contrast, MH treatment caused depletion of pathogenic bacteria namely, *Staphylococcus, Enterococcus,* and *Bacteroides.*

Next, we investigated if microbiota alteration induced by treatment was similar in MH versus SC groups. Significantly changed microbiota identified by LDA analysis in MH and SC groups (from Figure 10A, B) were compared, and Venn diagram (Figure 10C) was used to identify unique and shared genera. Most of the genera altered in response to treatment with MH and SC were unique for each group. Only two genera were shared between the two groups, namely *Methylarcula* (more in MH in week 4, and more in SC in week 0, i.e. enriched after treatment with MH and depleted after treatment with SC), and *Geovibrio* (less in week 4 in both groups, i.e. reduced due to treatment with both SC and MH). Moreover, we compared the genera detected in MH and SC groups after 4 weeks of treatment to explore microbiota differences between these groups post-treatment. As shown in Figure 10D, significant differences were found in the genera after 4 weeks of treatment with SC or MH (marked with asterisk in the heatmap). The LDA analysis of the significantly different genera is shown in Supplementary Figure 4 (sFigure 4). The heatmap also shows the genera with significant difference between week 0 and week 4 after each treatment (shown in figure 10A and B) and reveals the distinct microbiota fingerprints per group.

Additionally, we have explored the effect of MH and SC treatment on microbiota diversity. The difference was not statistically significant in alpha and beta diversity, but the only exception was seen in Shannon's index of richness and evenness. The latter index was significantly higher after treatment with MH for 4 weeks compared to the baseline in week 0. This effect was not evident after treatment with SC. Nevertheless, pairwise comparison between SC and MH in week 0 and week 4 did not reveal any significant difference between these groups. Comparison of alpha and beta diversity are shown in Supplementary Figures 5 and 6 (sFigure 5 and sFigure 6). Altogether, our findings demonstrate that MH treatment led to distinct changes in microbiota composition that are significantly different from the effect of SC, with identification of key microbiota that were increased or decreased following treatment.

DISCUSSION

Previous reports from our laboratory highlighted the role of MH as an anti-cancer and immunomodulatory agent [6,8–10,15,46]. In the current study, we present compelling evidence demonstrating the capacity of orally-administered MH to boost anti-tumor immune defense against an implanted colon adenocarcinoma tumor. To the best of our knowledge, this is the first report to demonstrate

mechanistically how preventative administration of MH can lead to alterations in the cellular landscape within the TME that promote a more effective anti-tumor immunity.

The present study highlights several novel findings regarding the potential use of MH as a preventative agent against cancer. First, *in vivo* experiments using the oral administration route demonstrated immunological alterations consistent with the induction of type I/II IFN signaling pathways. Second, the significance of MH-induced immunological alterations was highlighted in a murine CRC model, where pre-treating mice with a daily oral dose of MH over 4 weeks resulted in the retardation of the growth of implanted tumors. Third, MH-mediated tumor inhibition correlated with a series of cellular changes within the TME. Fourth, these intratumoral cellular alterations were accompanied by changes in the expression levels of various immunomodulatory chemokines and inflammatory cytokines. Lastly, MH treatment modulated gut microbiota composition, enriching for a unique pattern of several bacterial genera and inducing a depletion of pathogenic bacteria.

While the proportions of immune cells in the peripheral lymphoid tissues remained unaltered after MH treatment, there was a noticeable increase in their activation status, as evidenced by the upregulation of Sca-1 expression on lymphoid cells in the MLNs, ILNs, and spleens. Sca-1 is a type I interferon-inducible protein [35–37], that is upregulated as a result of inflammatory responses [47]. Thus, the data indicate that oral MH treatment triggers an inflammatory response that ultimately leads to an enrichment of type I interferons in both the gut and periphery. Induction of type I IFN is triggered when PAMPs interact with membrane-bound pathogen recognition receptors (PRRs), such as TLRs. TLRs recruit the MyD88 adaptor protein upon binding with their respective ligands, which leads to downstream activation of NF-kB, interferon regulatory factor 3 (IRF3), and interferon regulatory factor 7 (IRF7) transcription factors, which are responsible for inducing type I interferons [48,49]. Our previous findings showed that the immunostimulatory effect of MH following its intraperitoneal administration was significantly reduced in the absence of the MyD88 protein, indicating that TLRs may be involved in MH-triggered response [15]. Since TLRs are involved in inducing type I IFN, it is plausible that oral administration of MH stimulates type I IFN through a TLR-dependent pathway. However, further investigation is required to verify this hypothesis. Utilizing mice with known TLR defects would be useful in confirming this notion and elucidating the underlying mechanism in finer detail.

Alternatively, the enhancement in anti-tumor immune responses by MH could be related to the demonstrated changes in gut microbiota. Microbial dysbiosis is known to stimulate the host immune system, particularly T cell immune responses [50,51]. A previous study showed that an increase in Sca-1 expression on lymphoid cells in MLNs and peripheral tissues is linked to microbial dysbiosis in B cell-defective (BCD) mice. The dysbiosis in the gut mucosal environment leads to type I IFN enrichment in $CD8^+$ T cells, resulting in increased anti-tumor immunity [52]. Honey has been shown to acquire protective prebiotic effects due to the presence of oligosaccharides and polyphenols as major constituents [53,54]. MH was shown to improve the growth of probiotic bacteria while inhibiting the growth of pathogens [55]. Animal studies have shown that oral administration of 2.2g/kg (44 mg/mouse) of MH to mice for 4 weeks leads to alterations in the concentrations of short-chain fatty acids (SCFAs) [56]. In a

clinical study, the consumption of 20g of MH daily for 12 weeks did not yield any significant changes in gut microbiota. However, the authors postulated that the prebiotic effects of MH may have been masked by various factors such as the interaction with other dietary components, the storage conditions of honey, and the relatively low dosage of MH administered during the study [57]. In the current study, we demonstrate the capacity of orally-administered MH to induce significant changes in gut microbiota composition. It is worth noting that the dose used in our study is a comparatively higher dose than previously used (approximately 140 mg/mouse, equivalent to a human dose of 39.8 g).

We investigated the impact of oral MH treatment on implanted tumors. By focusing on using a preventative treatment regimen, we could delineate the immunomodulatory effect of MH from its anti-tumor effect. Our findings demonstrated a 44% reduction in tumor growth compared to the control group. To gain insights into the underlying mechanism of this effect, we analyzed the immune system components of CT26 tumors by flow cytometry. Our analysis revealed that the observed inhibition of tumor growth was associated with a significant enhancement in $CD45^+$ hematopoietic cell infiltration into the tumor tissue. Further investigation revealed that treatment with MH increased the proportion of intratumoral cytotoxic and helper T cells. T cells have been shown to play a crucial role in inducing anti-tumor immune responses [58]. Cytotoxic effector $CD8^+$ T cells can directly recognize and kill cancer cells by releasing cytotoxic molecules, such as granzymes and perforin, as well as pro-inflammatory cytokines like IFN-γ and TNF-α [59]. Similar to $CD8^+$ T cells, $CD4^+$ T cells secrete pro-inflammatory cytokines with direct anti-tumor effects [60]. Additionally, $CD4^+$ T cells play a crucial role in activating and expanding $CD8^+$ T cells through the secretion of IL-2, which promotes their proliferation and activation. Moreover, $CD4^+$ T cells license DCs to activate $CD8^+$ cells by either cross-presenting tumor antigens to $CD8^+$ T cells or inducing the production of cytokines and costimulatory molecules [61–63]. Our findings revealed that MH treatment not only increased the infiltration of intratumoral T cells but also enhanced their cytotoxic potential, as shown by the elevated levels of IFN-γ and granzyme-B in purified $CD45^+$ immune cells from tumor tissue.

In addition to alterations in TILs, we have observed changes in the intratumoral myeloid populations in response to MH treatment. Specifically, there was a reduction in the proportion of $CD11b^+$ myeloid cells, accompanied by a significant decrease in the proportion of $Ly6G^+$ granulocytes. In addition, MH treatment enhanced the antigen-presenting capacity of intratumoral myeloid cells, as evidenced by their increased expression of MHC class II proteins. Myeloid cells, including TAMs, DCs, TANs, and MDSCs, are the most abundant immune cells in the TME, and their heterogeneity allows them to exert both pro-tumor and anti-tumor effects during tumor development and progression [64]. The role of MDSCs in suppressing anti-tumor immunity and supporting the proliferation of tumors has been well-documented [38]. In our study, MH-mediated tumor inhibition was associated with a significant reduction in the percentages of intratumoral $Ly6G^+$ myeloid cells, which resemble granulocytic-MDSCs that are known to contribute to tumor growth promotion and immune response suppression. Various studies have reported the presence of granulocytic-MDSCs within the tumors and organs of CT26-bearing mice [38,65,66]. CT26 tumors produce proinflammatory mediators and factors that contribute to the

development and expansion of granulocytic-MDSCs in both primary tumors and distant organs [67,68]. This alteration in myeloid populations could explain the tumor-inhibiting effects of MH treatment. An increase in both the proportion and functional ability of cytotoxic T cells following MH treatment suggests that the suppressive effect of granulocytic-MDSCs on T cells is reduced. However, to verify this, it is crucial to directly evaluate the immunosuppressive capacity of intratumoral $Ly6G^+$ $CD11b^+$ cells by performing cellular function assays. Our results also indicated an increase in the expression of MHC-II proteins on the intratumoral myeloid cells, implying that type I and/or type II interferons could be responsible for this induction [33,34]. These findings indicate that these cells are potentially more able to act as antigen-presenting cells to $CD4^+$ helper T cells, hence augmenting anti-tumor T cell responses [58].

One major mechanism through which tumors avoid the immune response is by downregulating MHC class I, thereby decreasing their recognition and elimination by cytotoxic $CD8^+$ T cells [69]. A promising approach to enhance the efficacy of anti-tumor therapies involves restoring the expression of MHC class I through type I/II IFN stimulation [70]. In the current study, MH treatment enhanced the expression of MHC-I on the $CD45^-$ tumor cells, indicating the involvement of type I and/or type II interferons in this induction. The increase in MHC-I expression is consistent with the observed increase in TILs and IFNγ expression in MH-treated mice. The upregulation in CXCL10 expression, which is induced by IFN-γ, can regulate the recruitment of inflammatory T lymphocytes [42]. Our findings also demonstrated that MH treatment reduces CXCL2 expression, which plays a crucial role in recruiting intratumoral granulocytic MDSCs and promoting their pro-tumor immunosuppressive function [43,71]. These findings suggest that oral MH treatment enhances the immunogenicity of CT26 tumor cells, making them more susceptible to cytotoxic T cell-mediated killing.

In line with our findings, previous studies demonstrated the potential of natural products like polyphenols to restructure the immunosuppressive microenvironment of tumors and hinder tumor growth [72,73]. These natural products have been shown to downregulate the percentages of immunosuppressive cells, such as MDSCs, Tregs, and M2-MACs, while promoting the proportions and function of anti-tumor effector T cells like $CD8^+$ T cells, $CD4^+$ T cells, and NK cells [72–74]. Given that MH comprises a variety of polyphenols, it is perhaps not unreasonable to suggest that these bioactive substances contribute to the elicitation of the observed anti-tumor immune responses following MH treatment.

There is mounting evidence indicating that the gut microbiota plays a crucial role in cancer development and response to anti-cancer therapies [75,76]. Analysis of the gut microbiota of CRC patients has shown that certain bacteria, such as *Streptococcus gallolyticus*, *Fusobacterium nucleatum*, *Escherichia coli*, *Bacteroides fragilis,* and *Enterococcus faecalis*, are more prevalent in CRC patients compared to the normal population, while the levels of other genera like *Roseburia*, *Clostridium*, *Faecalibacterium* and *Bifidobacterium* decrease in CRC patients [77]. Experimental evidence from preclinical as well as clinical studies demonstrated that gut microbiota plays a critical role in influencing the response to anti-cancer therapies. For instance, in a murine melanoma model, the presence of commensal *Bifidobacterium* was

linked to differences in response to immune ICIs, and fecal microbiota transplantation (FMT) improved the anti-tumor effectiveness of PD-L1 blockade [78]. Clinical studies have further revealed that the composition and diversity of the gut microbiota can predict a favorable response to ICI immunotherapy, with specific bacterial strains such as *Ruminococcus*, *Akkermansia muciniphila*, and *Bifidobacterium* being present in the gut microbiome of ICI-responsive patients [79,80]. Therefore, manipulating the gut microbiome may have broad potential in cancer prevention and treatment.

Overall, our study indicates that oral administration of MH has the potential to activate the immune system and enhance anti-cancer immune responses in a preclinical model of CRC. Although the full mechanistic details remain unknown, our findings suggest that pretreatment with MH can activate lymphoid cells in mucosal and peripheral tissues, thereby facilitating a preactivated ready-to-respond state, that is most likely contributing to the superior anti-tumor immunity. MH appears to enrich for type I IFN signature by altering the gut microbiota, leading to the upregulation of Sca-1 on $CD4^+$ and $CD8^+$ cells in the gut, and their subsequent migration from the gut to the periphery. These T cells possess superior effector potential, ultimately promoting anti-tumor immune responses. The increased efficacy is linked to a series of immunological alterations within the TME, resulting in the suppression of tumor growth. The proposed mechanism of action for oral MH treatment is summarized in Figure 11.

Declarations

DATA AVAILABILITY STATEMENT

The data supporting the findings of this study are available within the article and its supplementary material. Further inquiries can be directed to the corresponding author.

ETHICS STATEMENT

The animal studies were reviewed and approved by the Institutional Animal Research Ethics Committee of the United Arab Emirates University.

AUTHOR CONTRIBUTIONS

B.K.a.-R. conceived the study and designed the experiments. R.J.M., G.B., A.A.-S., and Y.A.M. performed experiments and data acquisition. R.J.M. and B.K.a.-R. analyzed experimental data. R.J.M., and B.K.a.-R. wrote the manuscript. F.A.-M. analyzed the microbiota sequencing data, prepared the figures, and helped in writing the manuscript. A.A.-T. assisted in counting immunohistochemistry slides of tumor tissue sections. M.J.F.-C. provided scientific insights, supervised immunohistochemistry experiments, and edited the manuscript. B.K.a.-R. acquired the funding for the study and supervised the project. All authors approved the submitted version.

FUNDING

R.J.M. was supported through a scholarship from the College of Graduate Studies, United Arab Emirates University. This work was supported by grants from Zayed Center for Health Sciences (#31R025) and UAEU Program for Advanced Research ((#G00002993), Office of Research and Sponsored Projects, United Arab Emirates University, to B. K. al-Ramadi. Additional support was provided to B. K. al-Ramadi's lab by ASPIRE, the technology program management pillar of Abu Dhabi's Advanced Technology Research Council, via the ASPIRE Precision Medicine Research Institute Abu Dhabi (ASPIREPMRIAD) award grant #VRI-20-10 (21R098).

ACKNOWLEDGEMENTS

The authors wish to acknowledge the United Arab Emirates University for supporting this project and the College of Graduate Studies for the PhD student scholarship awarded to R.J.M. We thank Mr. Arshad Khan for excellent technical assistance and invaluable help in animal husbandry.

CONFLICT OF INTEREST

The authors declare that the research was conducted in the absence of any commercial or financial relationships that could be construed as a potential conflict of interest.

References

1. WHO. Cancer [Internet]. 2022. Available from: https://www.who.int/news-room/fact-sheets/detail/cancer

2. Thorsson V, Gibbs DL, Brown SD, Wolf D, Bortone DS, Ou Yang T-H, et al. The Immune Landscape of Cancer. Immunity. 2018;48:812-830.e14.

3. Schreiber RD, Old LJ, Smyth MJ. Cancer Immunoediting: Integrating Immunity's Roles in Cancer Suppression and Promotion. Science. 2011;331:1565–70.

4. Burnet. The Concept of Immunological Surveillance. Prog Exp Tumor Res. 1970. p. 1–27.

5. Dunn GP, Old LJ, Schreiber RD. The Three Es of Cancer Immunoediting. Annu Rev Immunol. 2004;22:329–60.

6. Afrin S, Haneefa SM, Fernandez-Cabezudo MJ, Giampieri F, al-Ramadi BK, Battino M. Therapeutic and preventive properties of honey and its bioactive compounds in cancer: an evidence-based review. Nutr

Res Rev. 2020;33:50–76.

7. Afrin S, Giampieri F, Forbes-Hernández TY, Gasparrini M, Amici A, Cianciosi D, et al. Manuka honey synergistically enhances the chemopreventive effect of 5-fluorouracil on human colon cancer cells by inducing oxidative stress and apoptosis, altering metabolic phenotypes and suppressing metastasis ability. Free Radic Biol Med. 2018;126:41–54.

8. Aryappalli P, Al-Qubaisi SS, Attoub S, George JA, Arafat K, Ramadi KB, et al. The IL-6/STAT3 Signaling Pathway Is an Early Target of Manuka Honey-Induced Suppression of Human Breast Cancer Cells. Front Oncol. 2017;7:167.

9. Fernandez-Cabezudo MJ, El-Kharrag R, Torab F, Bashir G, George JA, El-Taji H, et al. Intravenous Administration of Manuka Honey Inhibits Tumor Growth and Improves Host Survival When Used in Combination with Chemotherapy in a Melanoma Mouse Model. PLoS One. 2013;8:e55993.

10. Aryappalli P, Shabbiri K, Masad RJ, Al-Marri RH, Haneefa SM, Mohamed YA, et al. Inhibition of Tyrosine-Phosphorylated STAT3 in Human Breast and Lung Cancer Cells by Manuka Honey is Mediated by Selective Antagonism of the IL-6 Receptor. Int J Mol Sci. 2019;20:4340.

11. Masad RJ, Haneefa SM, Mohamed YA, Al-Sbiei A, Bashir G, Fernandez-Cabezudo MJ, et al. The Immunomodulatory Effects of Honey and Associated Flavonoids in Cancer. Nutrients. 2021;13:1269.

12. Chepulis LM, Francis E. An Initial Investigation into the Anti-inflammatory Activity and Antioxidant Capacity of alpha-Cyclodextrin-Complexed Manuka Honey. J Complement Integr Med. 2012;9.

13. Gasparrini M, Afrin S, Forbes-Hernández TY, Cianciosi D, Reboredo-Rodriguez P, Amici A, et al. Protective effects of Manuka honey on LPS-treated RAW 264.7 macrophages. Part 2: Control of oxidative stress induced damage, increase of antioxidant enzyme activities and attenuation of inflammation. Food and Chemical Toxicology. 2018;120:578–87.

14. Ahmed S, Sulaiman SA, Othman NH. Oral Administration of Tualang and Manuka Honeys Modulates Breast Cancer Progression in Sprague-Dawley Rats Model. Evidence-Based Complementary and Alternative Medicine. 2017;2017:1–15.

15. Masad RJ, Nasser RA, Bashir G, Mohamed YA, Al-Sbiei A, Al-Saafeen BH, et al. Characterization of immunomodulatory responses induced by manuka honey. Front Immunol. 2022;13:1020574.

16. Tonks AJ, Cooper RA, Jones KP, Blair S, Parton J, Tonks A. Honey stimulates inflammatory cytokine production from monocytes. Cytokine. 2003;21:242–7.

17. Tonks AJ, Dudley E, Porter NG, Parton J, Brazier J, Smith EL, et al. A 5.8-kDa component of manuka honey stimulates immune cells via TLR4. J Leukoc Biol. 2007;82:1147–55.

18. Tonks A, Cooper RA, Price AJ, Molan PC, Jones KP. Stimulation of TNF-α release in monocytes by honey. Cytokine. 2001;14:240–2.

19. Timm M, Bartelt S, Hansen EW. Immunomodulatory effects of honey cannot be distinguished from endotoxin. Cytokine. 2008;42:113–20.

20. Viaud S, Saccheri F, Mignot G, Yamazaki T, Daillère R, Hannani D, et al. The Intestinal Microbiota Modulates the Anticancer Immune Effects of Cyclophosphamide. Science. 2013;342:971–6.

21. Paulos CM, Wrzesinski C, Kaiser , Andrew, Hinrichs CS, Chieppa M, Cassard L, et al. Microbial translocation augments the function of adoptively transferred self/tumor-specific CD8+ T cells via TLR4 signaling. Journal of Clinical Investigation. 2007;117:2197–204.

22. al-Ramadi BK, Fernandez-Cabezudo MJ, El-Hasasna H, Al-Salam S, Attoub S, Xu D, et al. Attenuated Bacteria as Effectors in Cancer Immunotherapy. Ann N Y Acad Sci. 2008;1138:351–7.

23. al-Ramadi BK, Fernandez-Cabezudo MJ, El-Hasasna H, Al-Salam S, Bashir G, Chouaib S. Potent anti-tumor activity of systemically-administered IL2-expressing Salmonella correlates with decreased angiogenesis and enhanced tumor apoptosis. Clinical Immunology. 2009;130:89–97.

24. al-Ramadi BK, Adeghate E, Mustafa N, Ponery AS, Fernandez-Cabezudo MJ. Cytokine expression by attenuated intracellular bacteria regulates the immune response to infection: the Salmonella model. Mol Immunol. 2002;38:931–40.

25. Kaimala S, Mohamed YA, Nader N, Issac J, Elkord E, Chouaib S, et al. Salmonella-mediated tumor regression involves targeting of tumor myeloid suppressor cells causing a shift to M1-like phenotype and reduction in suppressive capacity. Cancer Immunology, Immunotherapy. 2014;63:587–99.

26. Al-Saafeen BH, Al-Sbiei A, Bashir G, Mohamed YA, Masad RJ, Fernandez-Cabezudo MJ, et al. Attenuated Salmonella potentiate PD-L1 blockade immunotherapy in a preclinical model of colorectal cancer. Front Immunol. 2022;13:1017780.

27. Fernández-Cabezudo MJ, Faour I, Jones K, Champagne DP, Jaloudi MA, Mohamed YA, et al. Deficiency of mitochondrial modulator MCJ promotes chemoresistance in breast cancer. JCI Insight. 2016;1.

28. Becker AAMJ, Munden S, McCabe E, Hurley D, Fanning S, Chapwanya A, et al. The Endometrial Microbiota—16S rRNA Gene Sequence Signatures in Healthy, Pregnant and Endometritis Dairy Cows. Vet Sci. 2023;10:215.

29. Hall M, Beiko RG. 16S rRNA Gene Analysis with QIIME2. 2018. p. 113–29.

30. Segata N, Izard J, Waldron L, Gevers D, Miropolsky L, Garrett WS, et al. Metagenomic biomarker discovery and explanation. Genome Biol. 2011;12:R60.

31. Chong J, Liu P, Zhou G, Xia J. Using MicrobiomeAnalyst for comprehensive statistical, functional, and meta-analysis of microbiome data. Nat Protoc. 2020;15:799–821.

32. Rahman B, Al-Marzooq F, Saad H, Benzina D, Al Kawas S. Dysbiosis of the Subgingival Microbiome and Relation to Periodontal Disease in Association with Obesity and Overweight. Nutrients. 2023;15:826.

33. Simmons DP, Wearsch PA, Canaday DH, Meyerson HJ, Liu YC, Wang Y, et al. Type I IFN Drives a Distinctive Dendritic Cell Maturation Phenotype That Allows Continued Class II MHC Synthesis and Antigen Processing. The Journal of Immunology. 2012;188:3116–26.

34. Steimle V, Siegrist C-A, Mottet A, Lisowska-Grospierre B, Mach B. Regulation of MHC Class II Expression by Interferon-γ Mediated by the Transactivator Gene CIITA. Science. 1994;265:106–9.

35. Khodadoust MM, Khan KD, Bothwell AL. Complex regulation of Ly-6E gene transcription in T cells by IFNs. J Immunol. 1999;163:811–9.

36. Snapper CM, Yamaguchi H, Urban JF, Finkelman FD. Induction of Ly-6A/E expression by murine lymphocytes after in vivo immunization is strictly dependent upon the action of IFN-α/β and /or IFN-γ. Int Immunol. 1991;3:845–52.

37. DeLong JH, Hall AO, Konradt C, Coppock GM, Park J, Harms Pritchard G, et al. Cytokine- and TCR-Mediated Regulation of T Cell Expression of Ly6C and Sca-1. The Journal of Immunology. 2018;200:1761–70.

38. Youn J-I, Nagaraj S, Collazo M, Gabrilovich DI. Subsets of Myeloid-Derived Suppressor Cells in Tumor-Bearing Mice. The Journal of Immunology. 2008;181:5791–802.

39. Qian B-Z, Li J, Zhang H, Kitamura T, Zhang J, Campion LR, et al. CCL2 recruits inflammatory monocytes to facilitate breast-tumour metastasis. Nature. 2011;475:222–5.

40. Van Overmeire E, Stijlemans B, Heymann F, Keirsse J, Morias Y, Elkrim Y, et al. M-CSF and GM-CSF Receptor Signaling Differentially Regulate Monocyte Maturation and Macrophage Polarization in the Tumor Microenvironment. Cancer Res. 2016;76:35–42.

41. Jongsma MLM, Guarda G, Spaapen RM. The regulatory network behind MHC class I expression. Mol Immunol. 2019;113:16–21.

42. Liu M, Guo S, Stiles JK. The emerging role of CXCL10 in cancer. Oncol Lett. 2011. p. 583–9.

43. Sawant K V., Sepuru KM, Lowry E, Penaranda B, Frevert CW, Garofalo RP, et al. Neutrophil recruitment by chemokines Cxcl1/KC and Cxcl2/MIP2: Role of Cxcr2 activation and glycosaminoglycan interactions. J Leukoc Biol. 2021;109:777–91.

44. Cullen SP, Brunet M, Martin SJ. Granzymes in cancer and immunity. Cell Death Differ. 2010;17:616–23.

45. Bhat P, Leggatt G, Waterhouse N, Frazer IH. Interferon-γ derived from cytotoxic lymphocytes directly enhances their motility and cytotoxicity. Cell Death Dis. 2017;8:e2836–e2836.

46. Masad RJ, Haneefa SM, Mohamed YA, Al-Sbiei A, Bashir G, Fernandez-Cabezudo MJ, et al. The immunomodulatory effects of honey and associated flavonoids in cancer. Nutrients. MDPI AG; 2021.

47. al-Ramadi BK, Al-Dhaheri MH, Mustafa N, AbouHaidar M, Xu D, Liew FY, et al. Influence of Vector-Encoded Cytokines on Anti- *Salmonella* Immunity: Divergent Effects of Interleukin-2 and Tumor Necrosis Factor Alpha. Infect Immun. 2001;69:3980–8.

48. Honda K, Takaoka A, Taniguchi T. Type I Inteferon Gene Induction by the Interferon Regulatory Factor Family of Transcription Factors. Immunity. 2006;25:349–60.

49. Kawai T, Akira S. The role of pattern-recognition receptors in innate immunity: update on Toll-like receptors. Nat Immunol. 2010;11:373–84.

50. Tanaka K, Sawamura S, Satoh T, Kobayashi K, Noda S. Role of the Indigenous Microbiota in Maintaining the Virus-Specific CD8 Memory T Cells in the Lung of Mice Infected with Murine Cytomegalovirus. The Journal of Immunology. 2007;178:5209–16.

51. Bachem A, Makhlouf C, Binger KJ, de Souza DP, Tull D, Hochheiser K, et al. Microbiota-Derived Short-Chain Fatty Acids Promote the Memory Potential of Antigen-Activated CD8+ T Cells. Immunity. 2019;51:285-297.e5.

52. Akrami M, Menzies R, Chamoto K, Miyajima M, Suzuki R, Sato H, et al. Circulation of gut-preactivated naïve CD8 $^{+}$ T cells enhances antitumor immunity in B cell-defective mice. Proceedings of the National Academy of Sciences. 2020;117:23674–83.

53. Mohan A, Quek S-Y, Gutierrez-Maddox N, Gao Y, Shu Q. Effect of honey in improving the gut microbial balance. Food Quality and Safety. 2017;1:107–15.

54. Schell KR, Fernandes KE, Shanahan E, Wilson I, Blair SE, Carter DA, et al. The Potential of Honey as a Prebiotic Food to Re-engineer the Gut Microbiome Toward a Healthy State. Front Nutr. 2022;9:957932.

55. Rosendale DI, Maddox IS, Miles MC, Rodier M, Skinner M, Sutherland J. High-throughput microbial bioassays to screen potential New Zealand functional food ingredients intended to manage the growth of probiotic and pathogenic gut bacteria. Int J Food Sci Technol. 2008;43:2257–67.

56. Rosendale D, Butts CA, de Guzman CE, Maddox IS, Martell S, McIntyre L, et al. Consumption of antimicrobial manuka honey does not significantly perturb the microbiota in the hind gut of mice. PeerJ. 2016;4:e2787.

57. Wallace A, Eady S, Miles M, Martin H, McLachlan A, Rodier M, et al. Demonstrating the safety of manuka honey UMF 20+in a human clinical trial with healthy individuals. Br J Nutr. 2010;103:1023–8.

58. Lei X, Lei Y, Li J-K, Du W-X, Li R-G, Yang J, et al. Immune cells within the tumor microenvironment: Biological functions and roles in cancer immunotherapy. Cancer Lett. 2020;470:126–33.

59. Farhood B, Najafi M, Mortezaee K. CD8+ cytotoxic T lymphocytes in cancer immunotherapy: A review. J Cell Physiol. 2019;234:8509–21.

60. Kennedy R, Celis E. Multiple roles for CD4 $^{+}$ T cells in anti-tumor immune responses. Immunol Rev. 2008;222:129–44.

61. Smith CM, Wilson NS, Waithman J, Villadangos JA, Carbone FR, Heath WR, et al. Cognate CD4+ T cell licensing of dendritic cells in CD8+ T cell immunity. Nat Immunol. 2004;5:1143–8.

62. Schoenberger SP, Toes REM, van der Voort EIH, Offringa R, Melief CJM. T-cell help for cytotoxic T lymphocytes is mediated by CD40–CD40L interactions. Nature. 1998;393:480–3.

63. Ridge JP, Di Rosa F, Matzinger P. A conditioned dendritic cell can be a temporal bridge between a CD4+ T-helper and a T-killer cell. Nature. 1998;393:474–8.

64. Dou A, Fang J. Heterogeneous Myeloid Cells in Tumors. Cancers (Basel). 2021;13:3772.

65. Masuda Y, Nakayama Y, Shimizu R, Naito K, Miyamoto E, Tanaka A, et al. Maitake α-glucan promotes differentiation of monocytic myeloid-derived suppressor cells into M1 macrophages. Life Sci. 2023;317:121453.

66. Liu Z, Xie Y, Xiong Y, Liu S, Qiu C, Zhu Z, et al. TLR 7/8 agonist reverses oxaliplatin resistance in colorectal cancer via directing the myeloid-derived suppressor cells to tumoricidal M1-macrophages. Cancer Lett. 2020;469:173–85.

67. Castle JC, Loewer M, Boegel S, de Graaf J, Bender C, Tadmor AD, et al. Immunomic, genomic and transcriptomic characterization of CT26 colorectal carcinoma. BMC Genomics. 2014;15:190.

68. Beury DW, Parker KH, Nyandjo M, Sinha P, Carter KA, Ostrand-Rosenberg S. Cross-talk among myeloid-derived suppressor cells, macrophages, and tumor cells impacts the inflammatory milieu of solid tumors. J Leukoc Biol. 2014;96:1109–18.

69. Cornel AM, Mimpen IL, Nierkens S. MHC Class I Downregulation in Cancer: Underlying Mechanisms and Potential Targets for Cancer Immunotherapy. Cancers (Basel). 2020;12:1760.

70. Lauss M, Donia M, Harbst K, Andersen R, Mitra S, Rosengren F, et al. Mutational and putative neoantigen load predict clinical benefit of adoptive T cell therapy in melanoma. Nat Commun. 2017;8:1738.

71. Hu J, Zhao Q, Kong L-Y, Wang J, Yan J, Xia X, et al. Regulation of tumor immune suppression and cancer cell survival by CXCL1/2 elevation in glioblastoma multiforme. Sci Adv. 2021;7.

72. Nuzzo G, Senese G, Gallo C, Albiani F, Romano L, d'Ippolito G, et al. Antitumor Potential of Immunomodulatory Natural Products. Mar Drugs. 2022;20:386.

73. Dong S, Guo X, Han F, He Z, Wang Y. Emerging role of natural products in cancer immunotherapy. Acta Pharm Sin B. 2022;12:1163–85.

74. Wang Q, Yang B, Wang N, Gu J. Tumor immunomodulatory effects of polyphenols. Front Immunol. 2022;13:1041138.

75. Wu M, Bai J, Ma C, Wei J, Du X. The Role of Gut Microbiota in Tumor Immunotherapy. J Immunol Res. 2021;2021:1–12.

76. Zhou C-B, Zhou Y-L, Fang J-Y. Gut Microbiota in Cancer Immune Response and Immunotherapy. Trends Cancer. 2021;7:647–60.

77. Cheng Y, Ling Z, Li L. The Intestinal Microbiota and Colorectal Cancer. Front Immunol. 2020;11:615056.

78. Sivan A, Corrales L, Hubert N, Williams JB, Aquino-Michaels K, Earley ZM, et al. Commensal *Bifidobacterium* promotes antitumor immunity and facilitates anti–PD-L1 efficacy. Science. 2015;350:1084–9.

79. Gopalakrishnan V, Spencer CN, Nezi L, Reuben A, Andrews MC, Karpinets T V., et al. Gut microbiome modulates response to anti–PD-1 immunotherapy in melanoma patients. Science. 2018;359:97–103.

80. Matson V, Fessler J, Bao R, Chongsuwat T, Zha Y, Alegre M-L, et al. The commensal microbiome is associated with anti–PD-1 efficacy in metastatic melanoma patients. Science. 2018;359:104–8.

Figures

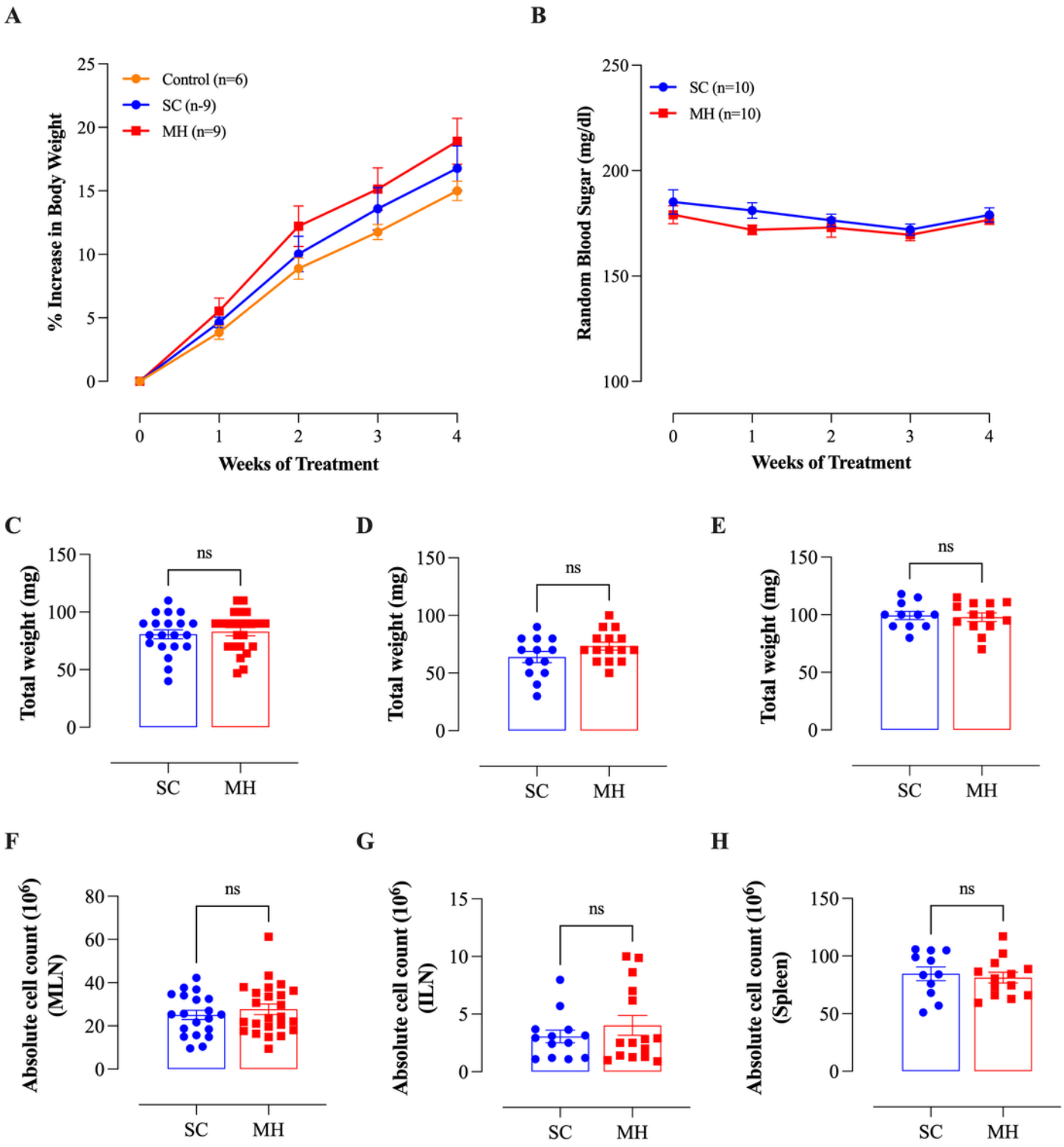

Figure 1

MH treatment does not alter the body weight, blood glucose levels, and the total weights and absolute cell counts of different peripheral lymphoid tissues. BALB/c mice were orally gavaged with filtered water, 70% SC or 70% MH for 4 consecutive weeks. Mice were then euthanized, and their MLNs, ILNs, and spleens were collected for further investigation. (**A**) Percent increase in body weight in mice treated with water, SC, or MH. Data is representative of 3 independent experiments. (**B**) Blood glucose levels of mice treated with

SC or MH. Data is pooled from 2 experiments. (**C-E**) Total weights (**C-E**) and absolute cell count (10^6) (**F-H**) of MLNs, ILNs, and spleens, respectively, following the treatment period. The values for individual mice and mean ± SEM are shown. Data in **(C, F)** is pooled from 5 independent experiments. Data in **(D, G)** is pooled from 4 independent experiments. Data in (**E, H**) is pooled from 3 independent experiments. p values were calculated using the unpaired Student's t-test, ns (no statistical significance, $p > 0.05$).

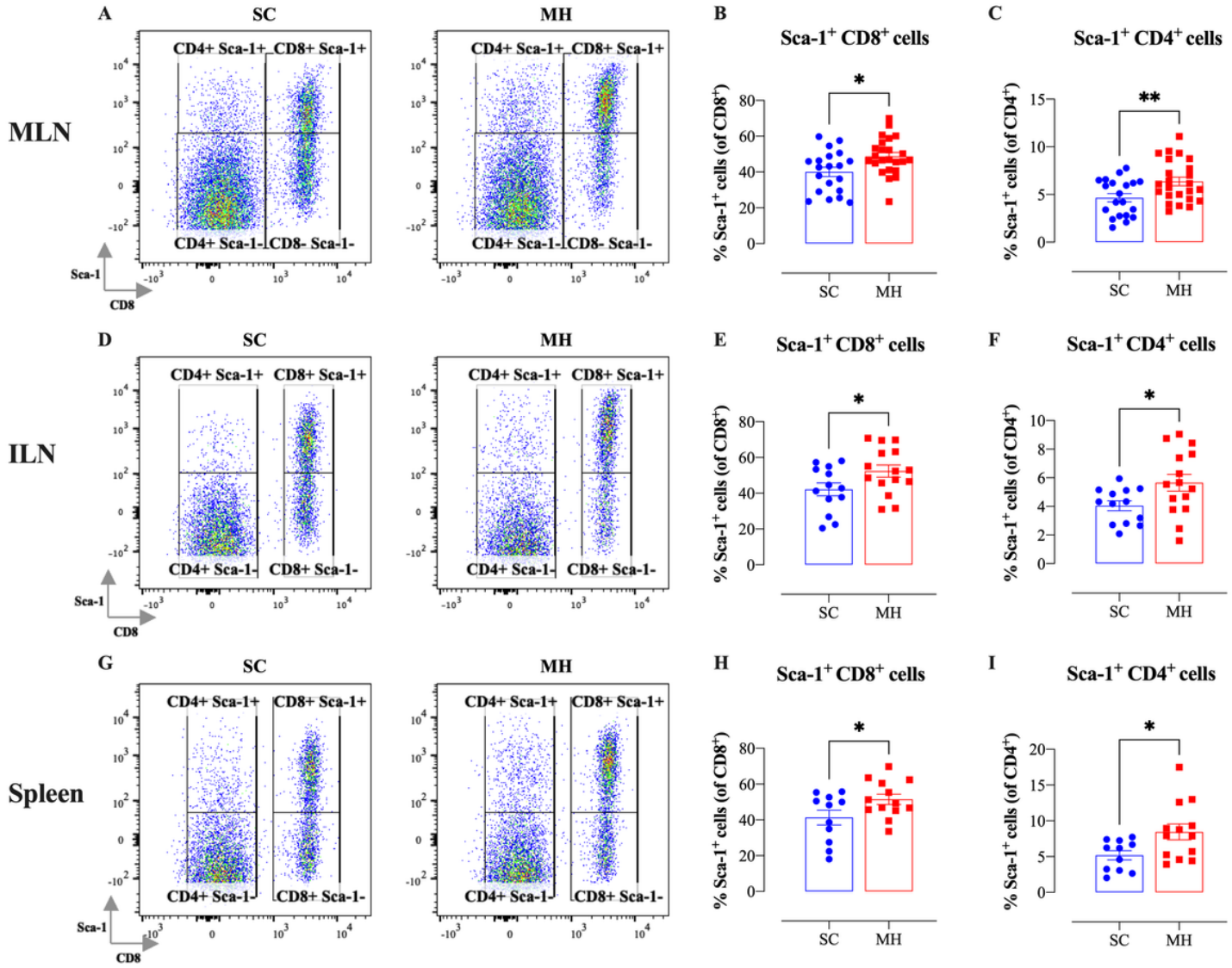

Figure 2

Lymphocyte activation in lymphoid tissues following MH treatment. BALB/c mice were orally gavaged with either SC or MH for 4 weeks. Following treatment, lymphoid organs were processed for flow cytometry analysis. Cells from MLNs (panels **A-C**), ILNs (panels **D-F**), and spleens (panels **G-I**) were analyzed to quantify the percentage of Sca-1^+ $CD8^+$ T cells (**B, E, H**), and Sca-1^+ $CD4^+$ T cells (**C, F, I**). Representative dot plots are shown in **A, D,** and **G**. The values for individual mice and mean ± SEM are shown. The data is pooled from 5 (**A-C**), 4 **(D-F)**, and 3 independent experiments **(G-I)**. p values were calculated using the unpaired Student's t-test, * ($p \leq 0.05$), and ** ($p \leq 0.01$).

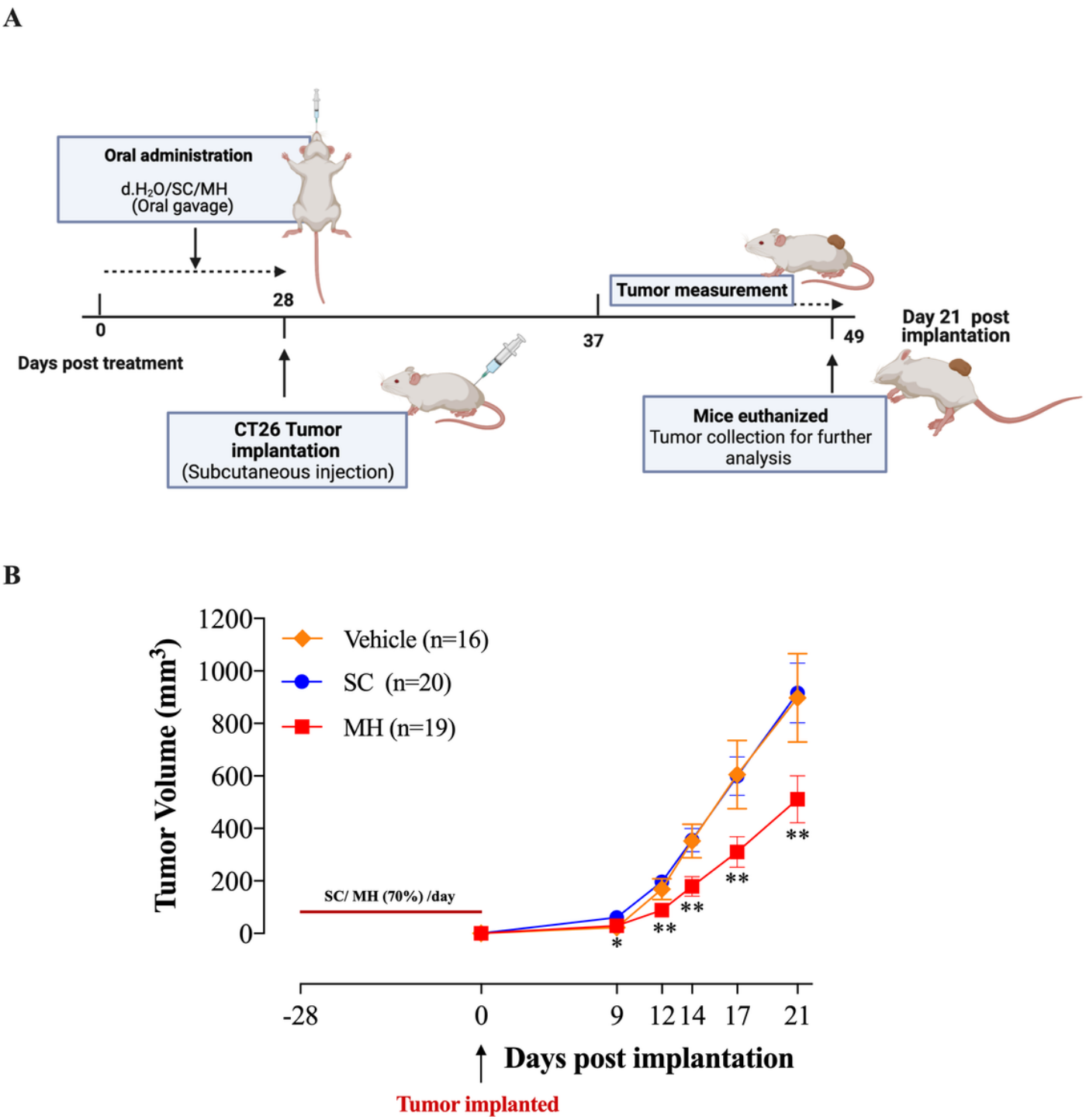

Figure 3

Oral MH treatment retards the growth of subsequently implanted CT26 tumors. (A) A schematic diagram describing the preventative model treatment protocol. BALB/c mice were orally gavaged daily with filtered water, 70% SC or 70% MH for 4 consecutive weeks. Following the treatment period, (2×10^5) CT26 CRC cells were subcutaneously implanted into the right flank of the mice, and tumor growth was followed for the subsequent 3 weeks. Mice were euthanized on day 21 post-implantation, and tumors were excised and processed for further analysis. **(B)** CT26 tumor growth of water-treated, SC-treated, and MH-treated

mice up to 21 days post-implantation. Each data point represents the mean ± SEM of 16-20 mice, pooled from 3 individual experiments. Asterisks denote statistically significant differences between the SC-treated and MH-treated groups. *p* values were calculated using the unpaired Student's t-test, * ($p \leq 0.05$), ** ($p \leq 0.01$).

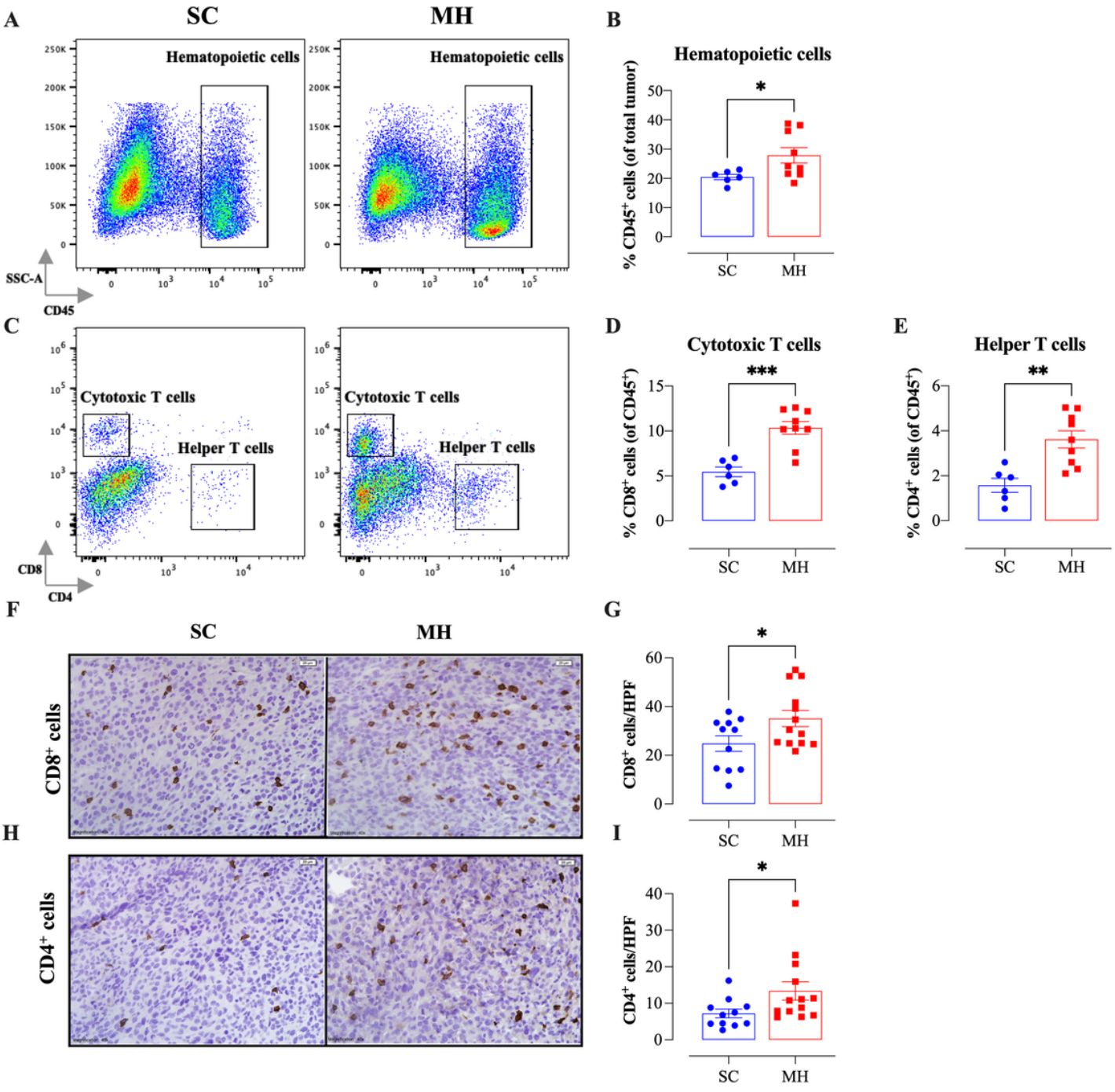

Figure 4

Increased tumor-infiltrating lymphocytes in MH-treated mice. BALB/c mice were orally gavaged with either 70% SC or 70% MH for 4 consecutive weeks, then implanted with CT26 tumor cells. Mice were euthanized on day 21 post-implantation, their tumors were resected, and the percentages of intratumoral

immune cells were determined by flow cytometry. (**A-E**) Representative flow plots, and the quantification of the percentages of $CD45^+$ immune cells (**A, B**), $CD8^+$ cytotoxic T cells (**C, D**), and $CD4^+$ helper T cells (**C, E**). The values for individual mice and mean ± SEM are shown (SC: n=6, MH: n=9), pooled from 2 independent experiments. **(F-I)** Tissue sections were analyzed by immunohistochemistry to quantify the number of $CD8^+$ and $CD4^+$ cells. Representative images at 40× magnification (scale bar 20 mm), and the quantitative estimation of the number of $CD8^+$ cells **(F, G)** and $CD4^+$ cells **(H, I)**/HPF (high-power field) are presented for each group. The values for individual mice and mean ± SEM are shown (SC: n=11, MH: n=13), pooled from 3 independent experiments. Asterisks denote statistically significant differences between the MH-treated and SC-treated groups. p values were calculated using the unpaired Student's t-test, * ($p \leq 0.05$), ** ($p \leq 0.01$), and *** ($p \leq 0.001$).

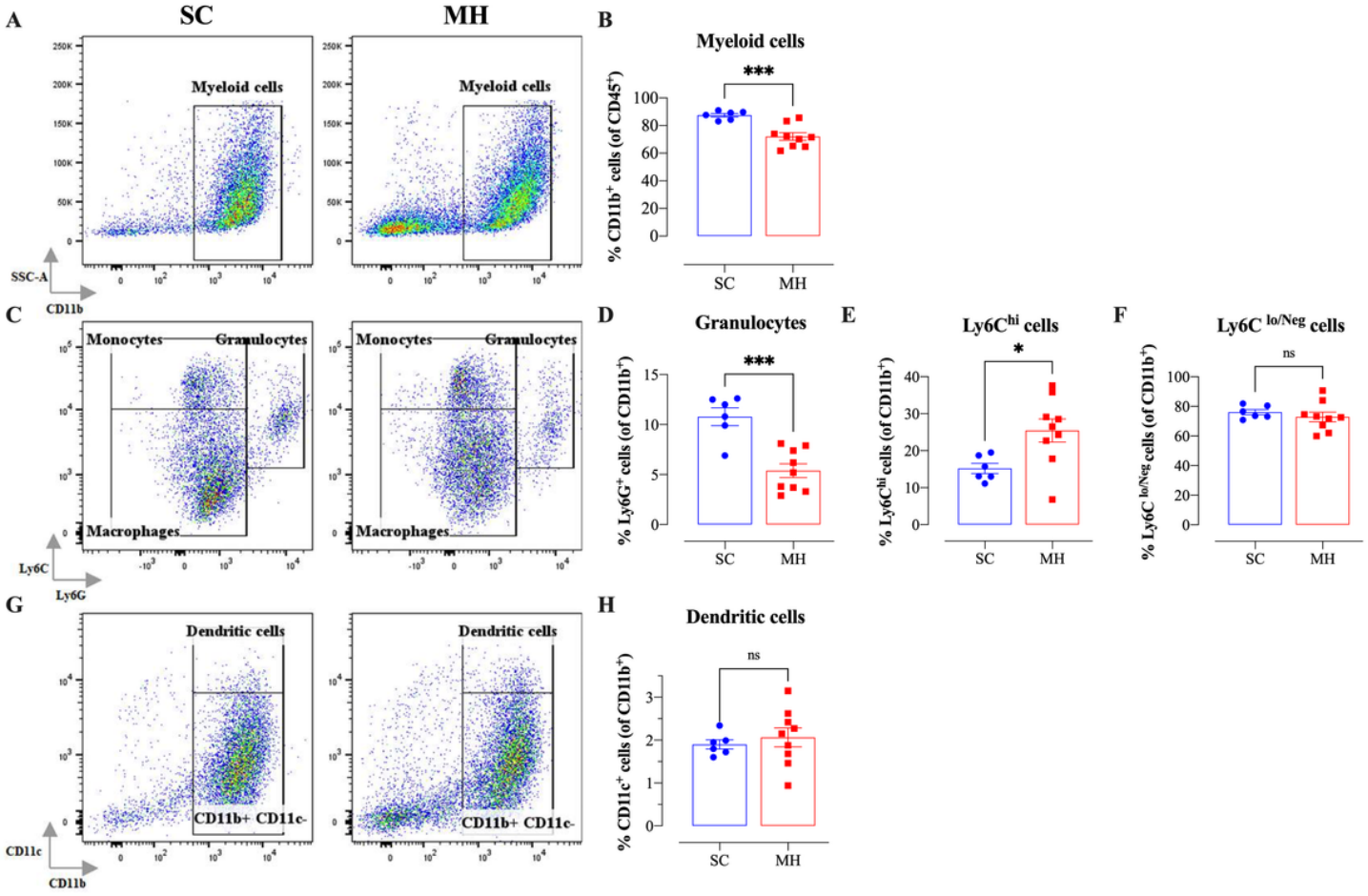

Figure 5

MH treatment alters intratumoral myeloid subpopulations. BALB/c mice were orally gavaged with either 70% SC or 70% MH for 4 consecutive weeks, then implanted with CT26 tumor cells. Mice were euthanized on day 21 post-implantation, their tumors were resected, and the percentages of intratumoral myeloid cells were determined by flow cytometry. (**A-H**) Representative flow plots, and the quantification of the percentages of $CD11b^+$ myeloid cells (**A, B**), $Ly6G^+$ granulocytes (**C, D**), $Ly6C^{hi}$ cells **(C, E)**, $Ly6C^{lo/Neg}$ cells **(C, F)**, and $CD11c^+$ dendritic cells **(G, H)**. The values for individual mice and mean ± SEM are shown (SC:

n=6, MH: n=9), pooled from 2 independent experiments. Asterisks denote statistically significant differences between the MH-treated and SC-treated groups. p values were calculated using the unpaired Student's t-test, * ($p \leq 0.05$), *** ($p \leq 0.001$), and ns (no statistical significance, $p > 0.05$).

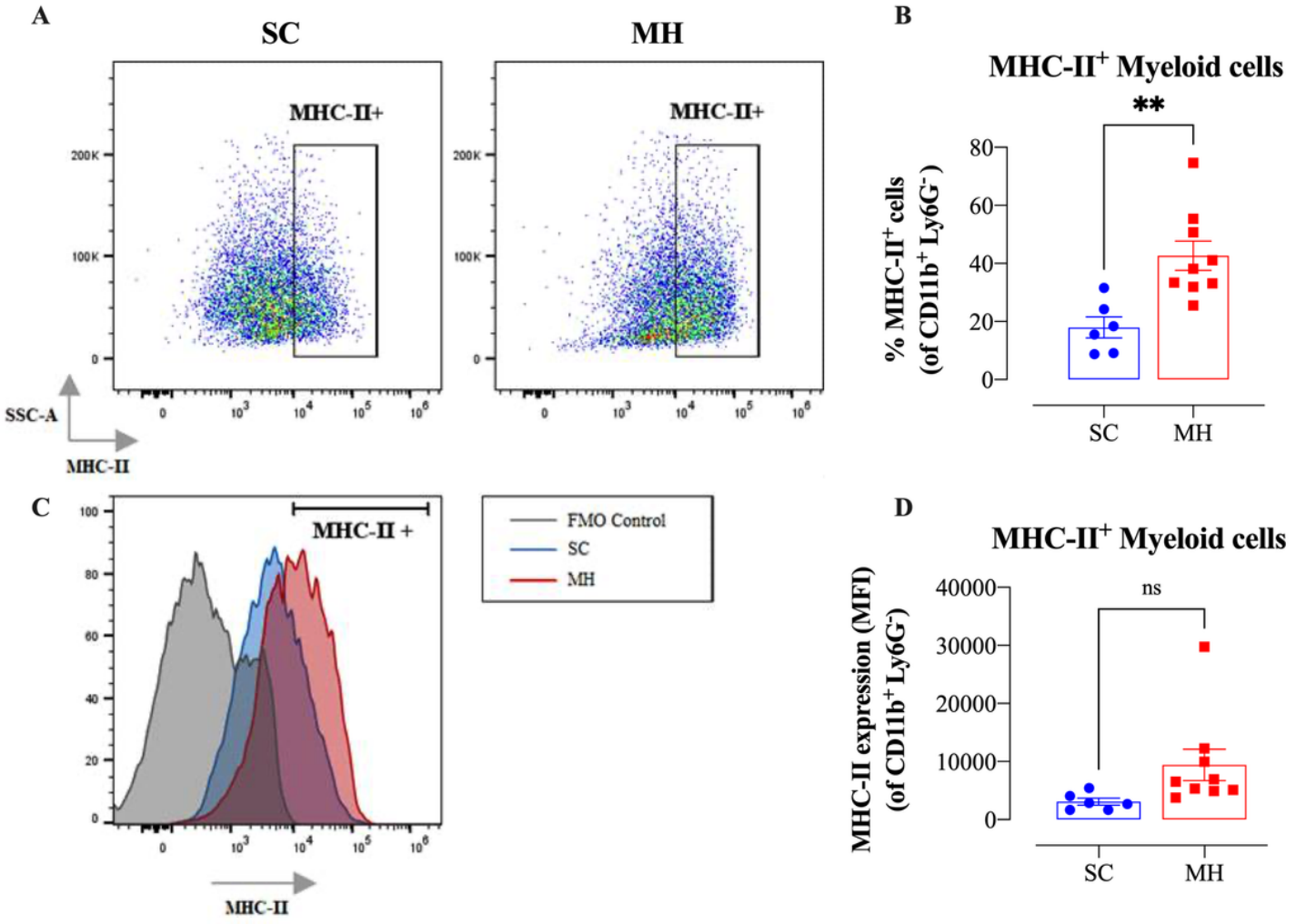

Figure 6

Upregulated expression of MHC class II proteins on intratumoral macrophages. BALB/c mice were orally gavaged with either 70% SC or 70% MH for 4 consecutive weeks, then implanted with CT26 tumor cells. Mice were euthanized on day 21 post-implantation, their tumors were resected, and processed for flow cytometry analysis. (**A-B**). Representative flow plots **(A),** and the quantification **(B)** of the percentage of MHC-II$^+$ cells (gated on CD11b$^+$ Ly6G$^-$ cells) in SC-treated and MH-treated mice. **(C)** Representative overlay histograms showing MHC-II expression on CD11b$^+$ Ly6G$^-$ myeloid cells of SC-treated and MH-treated mice. The grey histogram indicates staining with FMO control. **(D)** Median fluorescence intensity of MHC-II$^+$ CD11b$^+$ Ly6G$^-$ in SC-treated and MH-treated groups. The values for individual mice and mean ± SEM are shown (SC: n=6, MH: n=9), pooled from 2 independent experiments. Asterisks denote statistically significant differences between the MH-treated and SC-treated groups. p values were calculated using the unpaired Student's t-test, ** ($p \leq 0.01$), and ns (no statistical significance, $p > 0.05$).

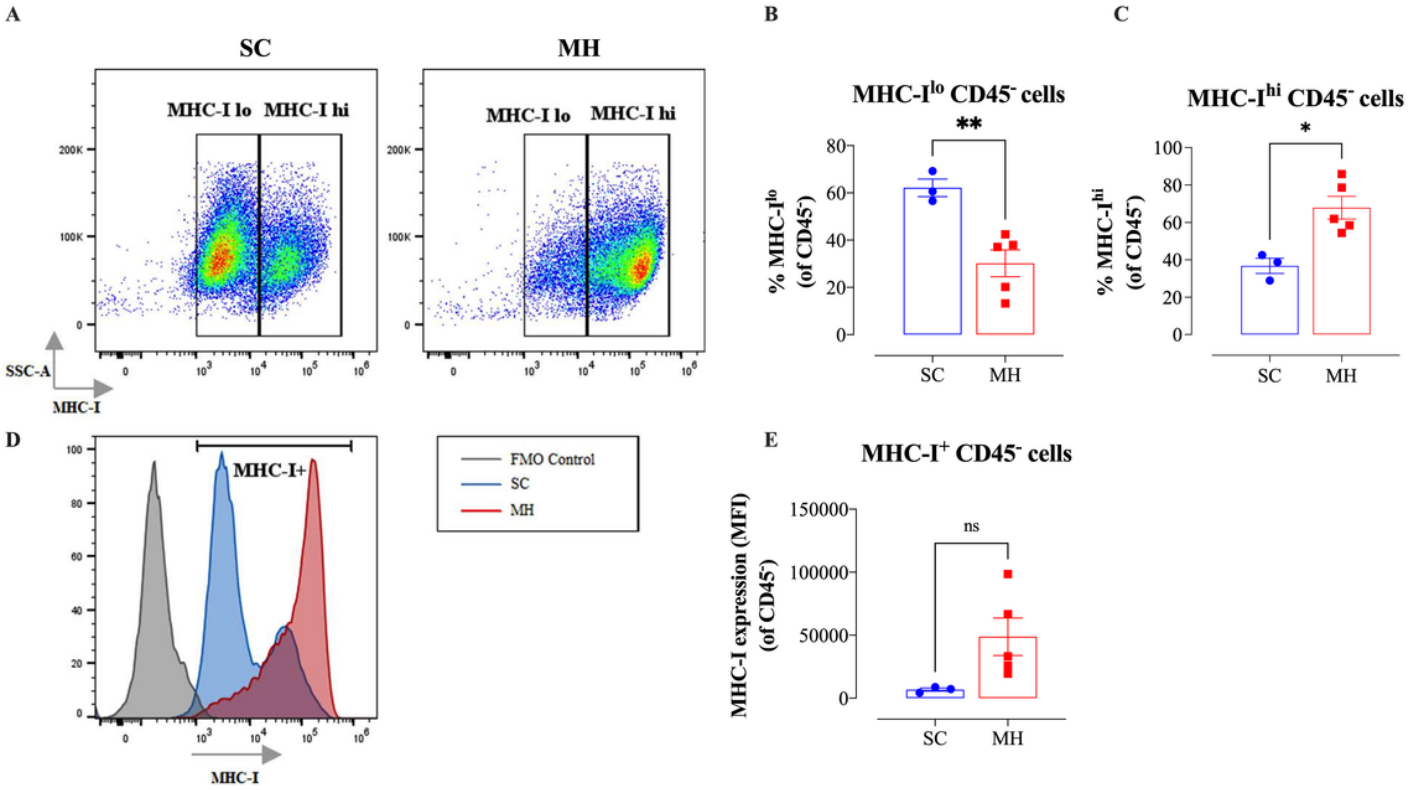

Figure 7

Enhancement in tumor immunogenicity as a consequence of MH administration. (**A-C**) Representative flow plots **(A)** and quantification of the percentage of MHC-I^{lo} **(B)** and MHC-I^{hi} **(C)** (gated on CD45$^-$ cells) in SC-treated and MH-treated mice. **(D)** Representative overlay histograms showing MHC-I expression on CD45$^-$ cells of SC-treated and MH-treated mice. The grey histogram indicates staining with FMO control (**E**) Median fluorescence intensity of MHC-I$^+$ CD45$^-$ cells in SC-treated and MH-treated groups. The values for individual mice and mean ± SEM are shown (SC: n=3, MH: n=5), obtained from 1 experiment. Asterisks denote statistically significant differences between MH-treated and SC-treated groups. p values were calculated using the unpaired Student's t-test, * ($p \leq 0.05$), ** ($p \leq 0.01$), and ns (no statistical significance, $p > 0.05$).

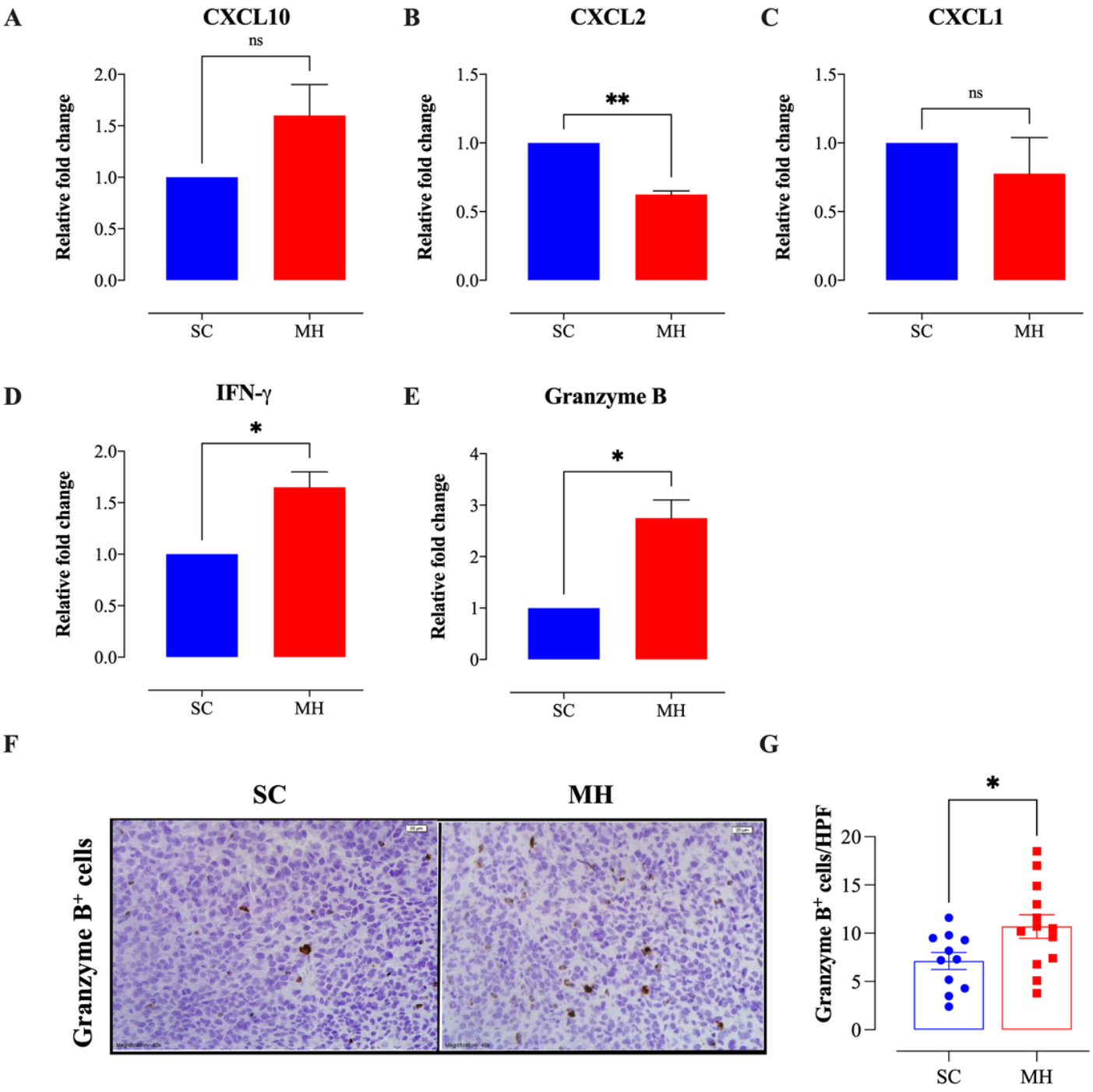

Figure 8

MH treatment alters the expression of chemokines and anti-tumor effector molecules. CT26 tumor tissues were excised from SC-treated and MH-treated mice on day 21 post-implantation. $CD45^+$ cells were purified from a pool of tumor cells obtained from 4 tumors per group. RNA was extracted from the purified $CD45^+$ cells and used to assess the mRNA levels of CXCL10 **(A)**, CXCL2 **(B)**, CXCL1 **(C)**, IFN-γ **(D)**, and granzyme B **(E)**. The data are expressed as means ± SEM of 2 replicates per group and are representative of 2 independent experiments. **(F, G)** Tissue sections were analyzed by immunohistochemistry to quantify the number of granzyme B^+ cells. Representative images at 40×

magnification (scale bar 20 mm) are presented for each group **(F)**. Quantitative estimation of the number of granzyme B^+ cells/ HPF (high-power field). The values for individual mice and mean ± SEM are shown (SC: n=11, MH: n=13), pooled from 3 independent experiments. Asterisks denote statistically significant differences between the MH-treated and SC-treated groups. p values were calculated using the unpaired Student's t-test, * ($p \leq 0.05$), ** ($p \leq 0.01$), and ns (no statistical significance, $p > 0.05$).

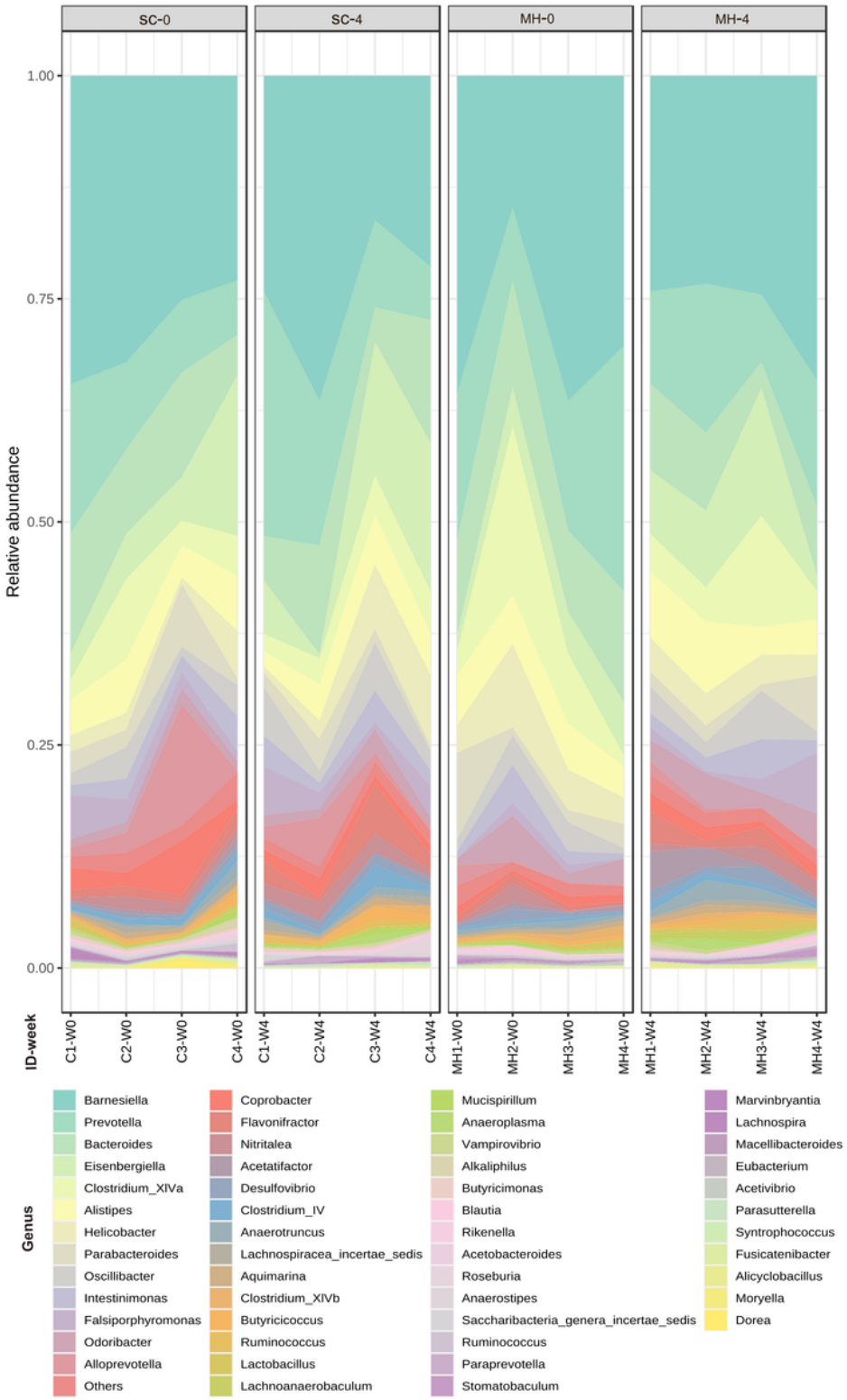

Figure 9

Relative abundance of genera detected at the baseline (week 0 before treatment) and in week 4 after treatment with SC or MH. Data shown represent the relative abundance of the genera listed, in each mouse investigated in this study before and after treatment.

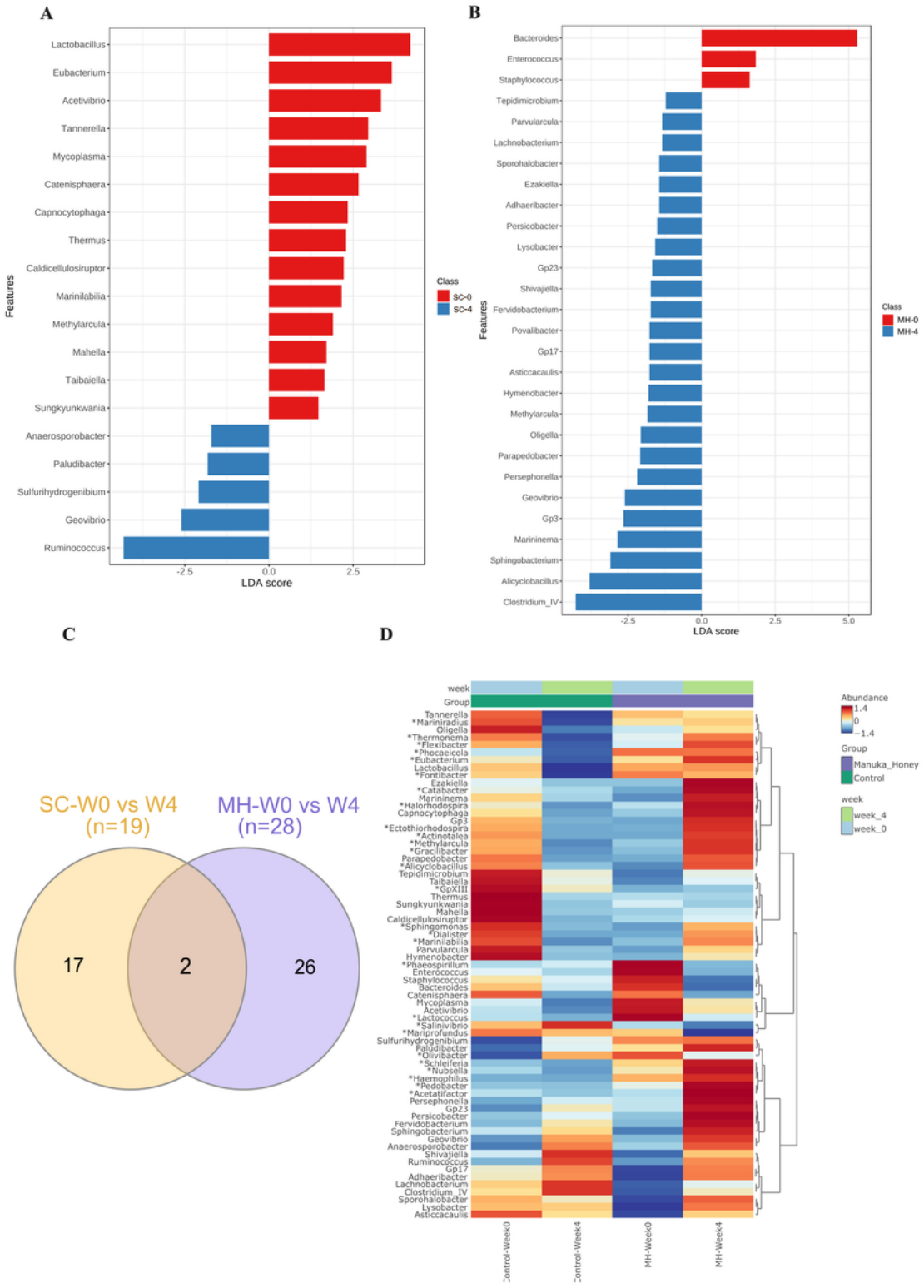

Figure 10

Microbiota variations after 4-week treatment. LDA analysis comparing genera pre and post-treatment with CS (A) and MH (B) showed depleted (red) and enriched (blue) in week 4 post-treatment. Venn diagram (C) of shared and unique genera that were significantly different pre- and post-treatment for each of the SC and MH groups. The heatmap (D) shows microbiota fingerprints in each group before and after treatment, with significantly altered genera. Asterisks (*) represent genera with significant differences between MH and CS after 4 weeks of treatment, while the rest are those with significant difference in week 0 compared to week 4 in either treatment group.

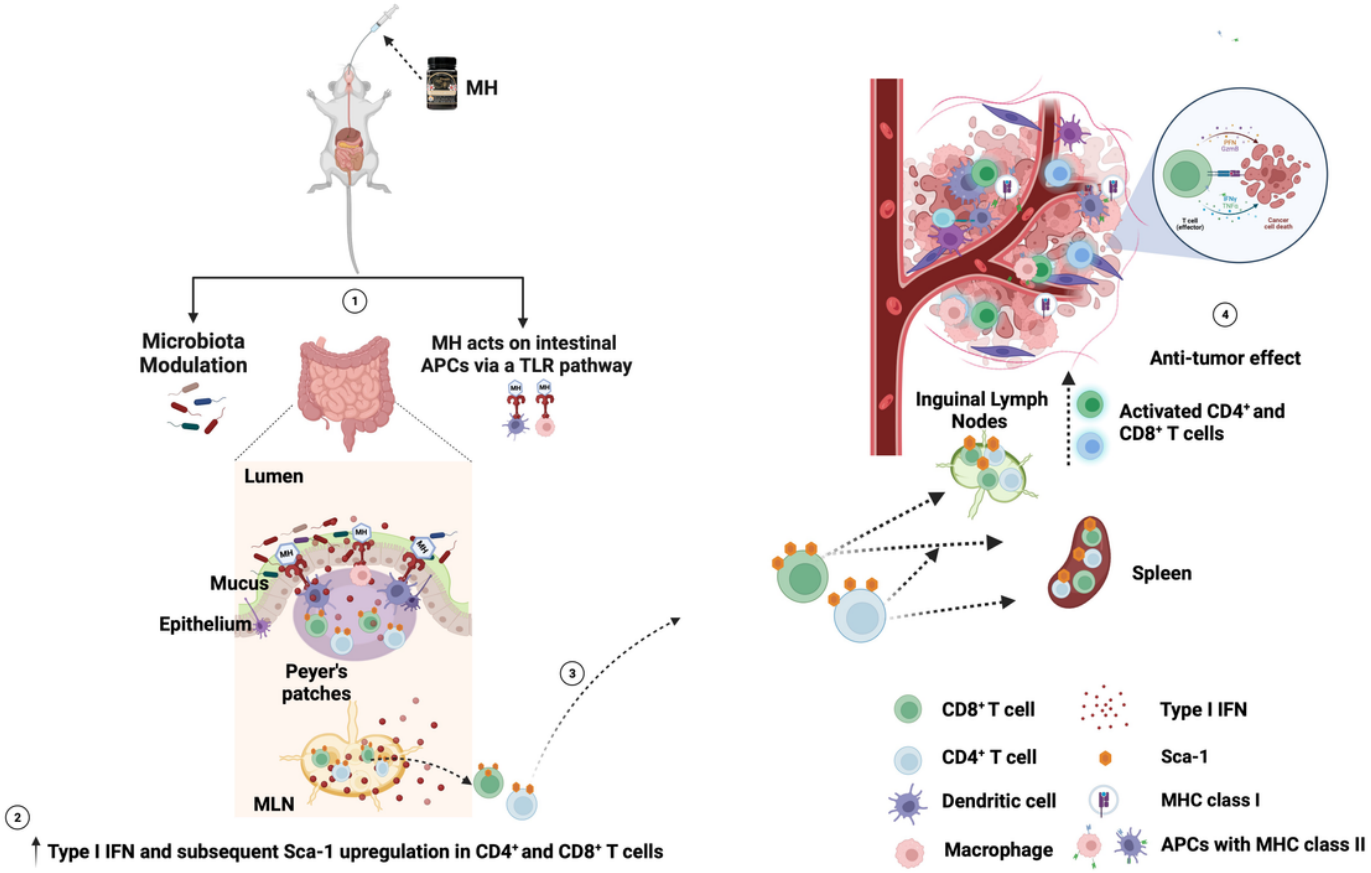

Figure 11

Schematic diagram of the proposed mechanism of oral treatment with MH and the subsequent anti-tumor immune response. **(1)** MH treatment either modulates the gut microbiota or induces the TLR pathway. This leads to **(2)** the enrichment of type I IFN and the subsequent upregulation of Sca-1 on the $CD4^+$ and $CD8^+$ T cells in the gut environment. **(3)** The Sca-1^+ $CD4^+$ and $CD8^+$ T cells migrate from the gut to the periphery (spleen and ILNs). **(4)** these preactivated T cells then migrate to the TME and induce anti-tumor immune responses. Figure adapted from [52] and created with BioRender.com.

Supplementary Files

This is a list of supplementary files associated with this preprint. Click to download.

- MasadetalSupplementaryFigures.pdf